



1
2
3
4
5
6
7
8
9
10
11
12
13
14
15
16
17
18
19
20
21
22
23
24
25
26
27
28
29
30
31
32
33
34
35
36
37
38
39

Widespread and Persistent Ozone Pollution in Eastern China

Guohui Li^{1*}, Naifang Bei², Junji Cao^{1*}, Jiarui Wu¹, Xin Long¹, Tian Feng^{1,2}, Wenting Dai¹, Suixin Liu¹, Qiang Zhang³, and Xuexi Tie¹

¹Key Lab of Aerosol Chemistry and Physics, SKLLQG, Institute of Earth Environment, Chinese Academy of Sciences, Xi'an, China

²School of Human Settlements and Civil Engineering, Xi'an Jiaotong University, Xi'an, Shaanxi, China

³Department of Environmental Sciences and Engineering, Tsinghua University, Beijing, China

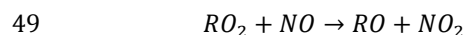
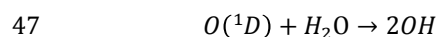
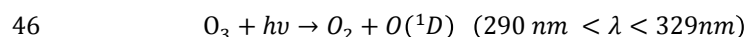
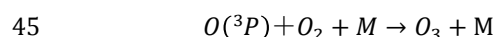
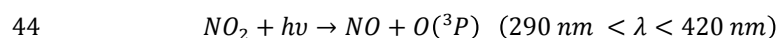
*Correspondence to: Guohui Li (ligh@ieecas.cn) and Junji Cao (jjcao@ieecas.cn)

Abstract: Rapid growth of industrialization, transportation, and urbanization has caused increasing emissions of ozone (O₃) precursors recently, enhancing the O₃ formation in Eastern China. We show here that Eastern China has experienced widespread and persistent O₃ pollution from April to September in 2015 based on the O₃ observations in 223 cities. The observed maximum 1-h O₃ concentrations exceed 200 μg m⁻³ in almost all the cities, 400 μg m⁻³ in more than 25% of the cities, and even 800 μg m⁻³ in six cities in Eastern China. The average daily maximum 1-h O₃ concentrations are more than 160 μg m⁻³ in 45% of the cities, and the 1-h O₃ concentrations of 200 μg m⁻³ have been exceeded on over 10% of days from April to September in 129 cities. A widespread and severe O₃ pollution episode from 22 to 28 May 2015 in Eastern China has been simulated using the WRF-CHEM model to evaluate the O₃ contribution of biogenic and various anthropogenic sources. The model generally performs reasonably well in simulating the temporal variations and spatial distributions of near-surface O₃ concentrations. Using the factor separate approach, sensitivity studies have indicated that the industry source plays the most important role in the O₃ formation, and constitutes the culprit of the severe O₃ pollution in Eastern China. The transportation source contributes considerably to the O₃ formation, and the O₃ contribution of the residential source is not significant generally. The biogenic source provides a background O₃ source, and also plays an important role in the south of Eastern China. Further model studies are needed to comprehensively investigate O₃ formation for supporting the design and implementation of O₃ control strategies, considering rapid changes of emissions inventories and photolysis caused by the ‘Atmospheric Pollution Prevention and Control Action Plan’, released by the Chinese State Council in 2013.



40 1 Introduction

41 In the urban planetary boundary layer (PBL), ozone (O_3) is formed as a result of
42 photochemical reactions involving volatile organic compounds (VOCs) and nitrogen oxide
43 (NO_x) in the presence of sunlight (Brasseur et al., 1999):



50 where hv represents the energy of a photo; $O(^3P)$ and $O(^1D)$ represent the ground state and
51 electronically excited oxygen atoms, respectively; RO_2 , RO , and OH denote peroxy, oxy, and
52 hydroxyl radicals, respectively. High O_3 concentrations ($[O_3]$) are of major environmental
53 concerns due to its deleterious impacts on ecosystems (e.g., National Research Council, 1991)
54 and human health (Lippman, 1993; Weinhold, 2008).

55 The emissions of O_3 precursors, VOCs and NO_x , have been significantly increased
56 recently in China due to rapid industrialization and urbanization, and increasing
57 transportation activity (e.g., Zhang et al., 2009; Kurokawa et al., 2013; Yang et al., 2015).
58 Satellite measurements have demonstrated that NO_x emissions have been increased by a
59 factor of 2 in Central and East China from 2000 to 2006 (Richter et al., 2005). Zhang et al.
60 (2009) have also shown an increasing trend of NO_x emissions with an enhancement of 55%
61 in China from 2001 to 2006. NO_x emissions have still continued to increase since 2006,
62 caused by increasing power plants and vehicles (Wang et al., 2012; Wang et al., 2013; Yang
63 et al., 2015). VOCs emissions have been estimated to increase by 29% during 2001 – 2006 in



64 China (Zhang et al., 2009), and predicted to increase by 49% by 2020 relative to 2005 levels
65 (Xing et al., 2011).

66 Increasing O₃ precursors emissions has caused O₃ to be one of the most serious air
67 pollutants of concern during summertime, particularly in Eastern China, including the North
68 China Plain (NCP), Yangtze River Delta (YRD), and Pearl River Delta (PRD) (e.g., Xu et al.,
69 2011; Tie et al., 2013; Li et al., 2013; Feng et al., 2016). For example, a maximum O₃
70 concentration of 286 ppb has been observed in urban plumes from Beijing (Wang et al.,
71 2006). Chen et al. (2015) have reported that the average maximum daily [O₃] exceed 150 µg
72 m⁻³ in the summer of 2015 at most of monitoring sites in Beijing. Wu et al. (2016) have also
73 shown that, during summertime of 2015 in Beijing, the average O₃ concentration in the
74 afternoon is 163.2 µg m⁻³, and the frequency of the O₃ exceedance with hourly [O₃]
75 exceeding 200 µg m⁻³ is 31.8%. In addition, Cheng et al. (2016) have demonstrated an
76 increasing trend of daily maximum 1-h [O₃] from 2004 to 2015 in Beijing, and Ma et al.
77 (2016) have reported significant increase of surface O₃ at a rural site in NCP. In PRD region,
78 the annual average near-surface O₃ level has been reported to increase from 24 ppbv in 2006
79 to 29 ppbv in 2009, and the maximum 1-h [O₃] can be up to 150 ~ 200 ppb in the summer
80 and fall (Ou et al., 2016, EST). Numerous studies have been performed to examine the severe
81 O₃ pollution in China, but primarily confined to mega-cities or industrial complexes. Few
82 studies have been conducted in whole Eastern China to investigate the O₃ pollution situation
83 and formation.

84 The China's Ministry of Environmental Protection (China MEP) has commenced to
85 release real-time hourly observations of pollutants, including O₃, NO₂, CO, SO₂, PM_{2.5}, and
86 PM₁₀ (particulate matter with aerodynamic diameter less than 2.5 and 10 µm, respectively)
87 since 2013. In Eastern China, there are 65 cities with air pollutants observations in 2013
88 during summertime, mainly concentrated in Beijing-Tianjin-Hebei (BTH), YRD, and PRD



89 (Figure 1). In 2015, a total of 223 cities have air pollutants observation in Eastern China,
90 providing a good opportunity to explore the O₃ pollution distributions. Therefore, in the
91 present study, the O₃ pollution situation in 2015 is first analyzed from April to September
92 when [O₃] are high in Eastern China. A high O₃ episode occurred in Eastern China in 2015 is
93 simulated using the WRF-CHEM model to evaluate the O₃ formation from biogenic and
94 various anthropogenic sources. The WRF-CHEM model configuration and methodology are
95 described in Section 2. Data analysis and model results are presented in Section 3, and
96 conclusions and discussions are given in Section 4.

97

98 **2 Model and Methodology**

99 **2.1 WRF-CHEM Model and Configurations**

100 In the present study, we use a specific version of the WRF-CHEM model (Grell et al.,
101 2005) to investigate the O₃ formation in Eastern China. The model is developed by Li et al.
102 (2010; 2011a, b; 2012) at the Molina Center for Energy and the Environment, including a
103 new flexible gas phase chemical module and the CMAQ/Models3 aerosol module developed
104 by US EPA (Binkowski and Roselle, 2003). The wet deposition of chemical species is
105 calculated using the method in the CMAQ module and the dry deposition parameterization
106 follows Wesely (1989). The FTUV is used to calculate photolysis rates (Tie et al., 2003; Li et
107 al., 2005), considering the impacts of aerosols and clouds on the photochemistry (Li et al.,
108 2011b). The ISORROPIA Version 1.7 is used to calculate the inorganic aerosols (Nenes et al.,
109 1998). The secondary organic aerosol (SOA) is predicted using a non-traditional SOA
110 module, including the volatility basis-set (VBS) modeling approach and SOA contributions
111 from glyoxal and methylglyoxal. Detailed information about the WRF-CHEM model can be
112 found in Li et al. (2010; 2011a, b; 2012).

113 A high O₃ pollution episode from 22 to 28 May 2015 in Eastern China is simulated



114 using the WRF-CHEM model. The simulation domain is shown in Figure 1. Detailed model
115 configurations are given in Table 1. For discussion convenience, Eastern China is divided
116 into four sections: 1) the Northeast China (including Heilongjiang, Jilin, Liaoning, and the
117 east part of Inner Mongolia, hereafter referred to as NEC), 2) the North China Plain and
118 surrounding areas (including Beijing, Tianjin, Hebei, Shandong, Henan, Shanxi, and the
119 north part of Jiangsu and Anhui, hereafter referred to as NCPs), 3) the YRD and surrounding
120 areas (including the south part of Jiangsu and Anhui, Shanghai, Zhejiang, and Hubei,
121 hereafter referred to as YRDs), and 4) the PRD and surrounding areas (including Fujian,
122 Jiangxi, Hunan, Guangxi, and Guangdong, hereafter referred to as PRDs) (shown in
123 Supplementary Information (SI), SI-Figure 1).

124 2.2 Statistical Methods for Comparisons

125 We use the mean bias (*MB*) and the index of agreement (*IOA*) to assess the WRF-
126 CHEM model performance in simulating air pollutants against measurements.

$$127 \quad MB = \frac{1}{N} \sum_{i=1}^N (P_i - O_i)$$

$$128 \quad IOA = 1 - \frac{\sum_{i=1}^N (P_i - O_i)^2}{\sum_{i=1}^N (|P_i - \bar{P}| + |O_i - \bar{O}|)^2}$$

129 where P_i and O_i are the calculated and observed pollutant concentrations, respectively. N is
130 the total number of the predictions used for comparisons, and \bar{P} and \bar{O} represents the average
131 of the prediction and observation, respectively. The *IOA* ranges from 0 to 1, with 1 showing
132 perfect agreement of the prediction with the observation.

133 2.3 Air Pollutants Measurements

134 The hourly near-surface CO, NO₂, SO₂, and PM_{2.5} mass concentrations from April to
135 September 2015 in Eastern China are released by China MEP, and can be downloaded from
136 the website <http://www.aqistudy.cn/>.

137

138 3 Results and Discussions



139 3.1 O₃ pollution in Eastern China

140 Continuous deterioration of air quality in China has engendered the implementation of
141 “Atmospheric Pollution Prevention and Control Action Plan” (hereafter referred to as
142 APPCAP), released by Chinese State Council in September 2013 to reduce PM_{2.5} by up to 25%
143 by 2017 relative to 2012 levels. Therefore, variations of air pollutants from 2013 to 2015
144 demonstrate the mitigation effects of implementation of the APPCAP on the air quality to a
145 considerable degree. A total of 65 cities, with 427 monitoring sites, have air pollutants
146 observations from 2013 to 2015 during April to September in Eastern China (Figure 1).
147 Considering the occurrence of high [O₃] in the afternoon (12:00 – 18:00 Beijing Time (BJT)),
148 Table 2 provides the average concentrations of air pollutants in the afternoon from April to
149 September in the 65 cities of Eastern China in 2013 and 2015. Apparently, implementation of
150 the APPCAP has decreased the mass concentrations of CO, SO₂, NO₂, and PM_{2.5} in Eastern
151 China, particularly with regard to SO₂, with a reduction of close to 40% from 2013 to 2015.
152 The [O₃] however exhibit an increasing trend, enhanced by 9.9% from 2013 to 2015.
153 Additionally, if the O₃ exceedance is defined as hourly [O₃] exceeding 200 μg m⁻³ (the
154 second grade of National Ambient Air Quality Standards in China), the O₃ exceedance
155 frequency in the afternoon has increased from 5.2% in 2013 to 6.8% in 2015, enhanced by
156 about 31.5%. There are several possible reasons for the O₃ pollution deterioration in Eastern
157 China since implementation of the APPCAP. Firstly, if the O₃ production regime in Eastern
158 China is NO_x-sensitive, the decrease of NO_x due to implementation of the APPCAP likely
159 enhances the O₃ formation. Secondly, mitigation of PM_{2.5} or aerosols directly or indirectly
160 increases the photolysis rates and expedites the O₃ formation. Thirdly, increasing
161 transportation activities enhances the emissions of VOCs and semi-VOCs, facilitating the O₃
162 formation. In addition, variability of meteorological situations also leads to the [O₃]



163 fluctuation. Hence, implementation of the APPCAP does not help mitigate $[O_3]$, and
164 unfortunately, severe O_3 pollutions have been looming in Eastern China.

165 In 2015, O_3 observations have been performed in 223 cities with 1064 monitoring sites
166 in Eastern China, which are used to analyze the O_3 pollution situation from April to
167 September. For comparisons, Figure 2 shows the distribution of observed maximum 1-h $[O_3]$
168 in Mainland China from April to September in 2015. The cities with the maximum 1-h $[O_3]$
169 exceeding $300 \mu\text{g m}^{-3}$ are mainly concentrated in NCPs, YRDs, and PRD. In Eastern China,
170 there are only two cities with the maximum 1-h $[O_3]$ less than $200 \mu\text{g m}^{-3}$. About 28% of
171 cities have observed more than $400 \mu\text{g m}^{-3}$ $[O_3]$ (about 200 ppb), showing widespread O_3
172 pollution in Eastern China. Furthermore, it is worth to note that the observed maximum 1-h
173 $[O_3]$ in six cities exceed $800 \mu\text{g m}^{-3}$ (about 400 ppb), in a very dangerous level.

174 Figure 3 presents the distribution of average daily maximum 1-h $[O_3]$ in Mainland
175 China from April to September 2015. The average daily maximum 1-h $[O_3]$ are more than
176 $120 \mu\text{g m}^{-3}$ in more than 95% of the cities, and $160 \mu\text{g m}^{-3}$ in 46% of the cities in Eastern
177 China. Particularly, there are seven cities with the average daily maximum 1-h $[O_3]$
178 exceeding $200 \mu\text{g m}^{-3}$ during six months. Figure 4 and 5 show the distributions of exceedance
179 days with the maximum 1-h $[O_3]$ exceeding 160 and $200 \mu\text{g m}^{-3}$ in Mainland China from
180 April to September 2015, respectively. There are more than 60 days with the maximum 1-h
181 $[O_3]$ exceeding $160 \mu\text{g m}^{-3}$ in 114 cities, and even more than 90 days in 62 cities in Eastern
182 China from April to September. The 1-h $[O_3]$ of $200 \mu\text{g m}^{-3}$ have been exceeded on over 10%
183 of days in 129 cities, and on 30% of days in 38 cities (Figure 5). Hence, persistent O_3
184 pollution has occurred in Eastern China from April to September in 2015.

185 Furthermore, in the urban PBL, high $[O_3]$ generally take place under calm or stable
186 circumstances with strong solar radiation. From April to September, the East Asian summer
187 monsoon influences Eastern China, causing intensified precipitation which inhibits the high



188 O₃ formation through washing out O₃ precursors and decreasing photolysis rates. So if
189 excluding rainy days in the analysis, the O₃ pollution becomes more severe in Eastern China.
190 For example, in Beijing, there are 54 rainy days and 65 days with the maximum 1-h [O₃]
191 exceeding 200 µg m⁻³ from May to August in 2015. If it does not rain in Beijing, the
192 occurrence possibility of the maximum 1-h [O₃] exceeding 200 µg m⁻³ is around 94%,
193 showing severe and persistent O₃ pollution.

194 3.2 Model Performance

195 The hourly measurements of O₃ and NO₂ in Eastern China are used to validate the
196 WRF-CHEM model simulations. Figure 6 presents the distributions of calculated and
197 observed near-surface [O₃] along with the simulated wind fields at 15:00 BJT from 22 to 27
198 May 2015. On May 22, Eastern China is influenced by the subtropical high whose center
199 locates over the Yellow sea. The east winds in the south of the high transport humid air into
200 PRDs, causing rainfall weather that substantially decreases [O₃]. The WRF-CHEM model
201 well reproduces the observed low [O₃] in the south of PRDs. In NCPs and YRDs, calm winds,
202 clear sky, and high temperature, induced by the high, facilitate the O₃ formation, and the
203 simulated [O₃] generally exceed 160 µg m⁻³, which is consistent with the observations. On
204 May 23, the subtropical high moves northward, also causing the rainfall belt in the south of
205 PRDs to extend northward. The simulated O₃ pollution in NCPs is deteriorated and also
206 extended to NEC, in good agreement with the measurements. From May 24 to 25, the
207 stagnant subtropical high continuously deteriorates the O₃ pollution in Eastern China. The
208 simulated and observed O₃ pollution on May 25 is widespread almost in Eastern China, and
209 the Northwest China also experiences high O₃ pollution. On May 26 and 27, the subtropical
210 high moves northward again and the rainfall belt has advanced to the south of NCPs. The
211 simulated and observed [O₃] in the north of NCPs and NEC are still high, but PRDs and
212 YRDs, the [O₃] have been significantly decreased due to precipitation. Generally, the



213 simulated O_3 spatial patterns are consistent with observations, but the model underestimation
214 or overestimation still exists. For example, the model remarkably overestimates the observed
215 $[O_3]$ on May 24, and also cannot well reproduce the high $[O_3]$ on May 25 in PRD. There are
216 several reasons for the model biases in simulating $[O_3]$ distribution. Firstly, the
217 meteorological situations play a key role in air pollution simulations (Bei et al., 2010, 2012),
218 determining the formation, transformation, diffusion, transport, and removal of the air
219 pollutants. Therefore uncertainties in meteorological fields simulations significantly influence
220 the air pollutants simulations. On May 24, the model fails to predict the rainy or overcast
221 weather, leading to remarked overestimation of $[O_3]$ in PRD. Secondly, the 10 km horizontal
222 resolution is used in simulations, which cannot resolve well cumulus clouds. The model
223 overestimates the $[O_3]$ observed in some cities with $[O_3]$ much lower than their surrounding
224 cities, which is primarily caused by the model failure in resolving convections. Thirdly, the
225 fast changes in emissions are not reflected in the emissions inventories used in the present
226 study.

227 Figure 7 provides the diurnal profiles of calculated and observed near-surface $[O_3]$
228 averaged over the ambient monitoring sites in provinces and municipalities in Eastern China
229 during the episode. The model reasonably well reproduces the temporal variations of surface
230 $[O_3]$ compared to observations, e.g., peak $[O_3]$ in the afternoon due to active photochemistry
231 and low $[O_3]$ during nighttime caused by the NO_x titration. Three provinces in NEC, Jilin,
232 Liaoning, and Inner Mongolia, are apparently impacted by the trans-boundary transport from
233 NCPs when the south winds are prevailing (Figure 6). So the uncertainties of wind field
234 simulations constitute one of the most important reasons for the model biases in modeling
235 $[O_3]$ in these three provinces. The model underestimates considerably the observed $[O_3]$ in
236 the three provinces (Figures 7a, c, d), with MBs exceeding $19 \mu g m^{-3}$. The model generally
237 exhibits good performance in simulating $[O_3]$ variations in the provinces of NCPs (Figures



238 7e-l) with *IOAs* exceeding 0.90, but is subject to underestimate the observations, particularly
239 in Beijing which is also significantly influenced by the trans-boundary transport (Wu et al.,
240 2016). In YRDs, the model cannot well predict the observed $[O_3]$ in Shanghai, which is
241 affected by the sea breeze when the large-scale wind fields are weak. In general, however,
242 current numerical weather prediction models, even in research mode, still have difficulties in
243 producing the location, timing, depth, and intensity of the sea-breeze front (Banta et al.,
244 2005). The model reasonably predicts the $[O_3]$ variations compared to measurements in PRDs
245 (Figures 7p-t) with *IOAs* more than 0.7, but overestimates the observed $[O_3]$ with *MBs*
246 varying from 3.8 to 16.7 $\mu\text{g m}^{-3}$, showing model biases in modeling precipitation processes.

247 The comparisons of simulated vs. observed distributions and temporal variations of
248 NO_2 mass concentrations ($[\text{NO}_2]$) are shown in Supplementary Information (SI, SI-Figures 2
249 and 3). The simulated high near-surface $[\text{NO}_2]$ are mainly concentrated in NCP, YRD, and
250 PRD, which is generally consistent with the measurements. The model also reasonably yields
251 temporal variations of $[\text{NO}_2]$ compared to measurements, but the simulations of $[\text{NO}_2]$ are
252 not as good as those of $[O_3]$, and the *IOAs* in Liaoning, Tianjin, and Shanghai are lower than
253 0.5. The difference between simulations and observations are frequently rather large during
254 nighttime, which perhaps caused by the model biases in modeling nighttime PBL or the
255 complexity of nighttime chemistry. In general, the calculated distributions and variations of
256 $[O_3]$ and $[\text{NO}_2]$ are consistent with the corresponding observations, showing that the
257 simulations of meteorological fields and emissions inventories are reasonable, providing the
258 base for sensitivity studies.

259 3.3 Sensitivity Studies

260 O_3 formation in the PBL is a complicated nonlinear process, depending on its
261 precursors of NO_x and VOCs from biogenic and various anthropogenic sources. It is
262 imperative to evaluate the O_3 contribution from various sources for devising the O_3 control



263 strategy. Rapid growth of industries, transportation, and urbanization has caused increasing
264 emissions of NO_x and VOCs in Eastern China (e.g., Zhang et al., 2009; Huang et al., 2011;
265 Wang et al., 2012; Wang et al., 2013; Yang et al., 2015). Numerous studies have also
266 demonstrated that biogenic VOCs, such as isoprene and monoterpenes, play a considerable
267 role in the O₃ formation in the PBL (e.g., Chameides et al., 1988; Tao et al., 2003; Li et al.,
268 2007; 2014). Therefore, sensitivity studies are used to evaluate the O₃ contributions of
269 biogenic, industry, residential, and transportation sources in Eastern China, respectively. It is
270 worth to note that emissions of power plants are directly associated with residential living
271 and industrial activities. So in the study, 75% of emissions from power plants are assigned to
272 the industry source and the rest are assigned to the residential source according to the ratio of
273 the power consumption used in industrial activities to residential living (Wang et al., 2016).

274 The factor separation approach (FSA) is used to evaluate the contribution of some
275 emission source to the O₃ concentration by differentiating two model simulations: one with
276 all emissions sources and the other without some emission source. Therefore, except the
277 control simulations with all emissions, additional four sensitivity simulations are performed,
278 in which the biogenic, industry, residential, and transportation emissions are excluded,
279 respectively, to assess their corresponding contributions to the O₃ formation in Eastern China.

280 Figure 8 shows the contribution of near-surface [O₃] averaged in the afternoon during
281 the whole episode from industry, residential, transportation, and biogenic emissions. The
282 industry source plays a more important role in the O₃ formation than the rest three sources,
283 with the O₃ contribution of 10 ~ 50 μg m⁻³ in the afternoon in Eastern China. In highly
284 industrialized areas, such as Hebei, Tianjin, Shandong, Zhejiang, et al., the O₃ contribution of
285 the industry source exceeds 30 μg m⁻³. The residential source is not important in the O₃
286 formation, and contributes about 2 ~ 15 μg m⁻³ O₃ generally. The transportation source plays
287 a considerable role in the O₃ formation, accounting for about 5 ~ 30 μg m⁻³ O₃ in Eastern



288 China. The O₃ enhancement due to biogenic emissions is mainly concentrated in NCPs and
289 PRDs, particularly in PRDs, with the O₃ contribution of around 5 ~ 50 μg m⁻³.

290 In order to further evaluate the contribution of various sources to the [O₃], the hourly
291 near-surface [O₃] in the control simulation are first subdivided into 16 bins with the interval
292 of 20 μg m⁻³. [O₃] in the control and sensitivity simulations as the bin [O₃] are assembled
293 respectively, and an average of [O₃] in each bin are calculated. Figures 9 shows the
294 contributions of various emissions sources to [O₃] in the four sections of Eastern China
295 during the episode. The industry emission plays the most important role in the O₃ formation,
296 and is the culprit of the high O₃ pollution. When the [O₃] in the control simulation are less
297 than 100 μg m⁻³, the industry source generally decreases [O₃]. However, when the simulated
298 [O₃] are more than around 200 μg m⁻³, the O₃ contribution from the industry emissions
299 generally exceeds 50 μg m⁻³, and when the simulated [O₃] are more than 300 μg m⁻³, the
300 industrial O₃ contribution can be up to 100 μg m⁻³, constituting one third of the [O₃]. The O₃
301 contribution from the residential source is not significant, generally less than 20 μg m⁻³. The
302 transportation source plays the second most important role in the O₃ formation in NEC, NCPs,
303 and YRDs, but its O₃ contribution is much less than that from the industry source when the
304 simulated [O₃] are more than 150 μg m⁻³. VOCs from the biogenic source generally enhance
305 the O₃ formation, providing a background O₃ source. The biogenic source contributes about
306 10 ~ 50 μg m⁻³ O₃ when simulated [O₃] are more than 150 μg m⁻³ in NEC, NCPs, and YRDs.
307 However, in PRDs, the biogenic emissions constitute the second most important O₃ source,
308 with the O₃ contribution exceeding 50 μg m⁻³ when simulated [O₃] are more than 250 μg m⁻³.
309 Apparently, controlling the industry emissions can substantially mitigate the severer O₃
310 pollution in Eastern China. If the industry emissions are not considered in model simulations,
311 on average, the [O₃] are generally not more than 200 μg m⁻³ in NEC, YRDs, and PRDs, but
312 still can exceed 160 μg m⁻³. In addition, excluding the industry source in NCPs does not



313 mitigate $[O_3]$ as remarkably as in the other regions, indicating that other emission sources
314 also play an important role in the O_3 formation. Although the transportation emission is the
315 second most important O_3 source in NEC, NCPs, and PRDs, its O_3 contribution is much less
316 than that from the industry source.

317 Another three sensitivity studies are conducted to further explore the high O_3 formation
318 in Eastern China, in which only the industry, residential, and transportation source is
319 considered, respectively. It is worth to note that biogenic emissions are included in all the
320 three sensitivity simulations considering that the biogenic emissions provide natural O_3
321 precursors and cannot be anthropogenically controlled. Figure 10 presents the O_3
322 contributions from individual anthropogenic source averaged in the afternoon during the
323 whole episode in the four sections of Eastern China. If only the industry source is considered
324 or the residential and transportation sources are excluded in the simulation, Eastern China
325 still experiences high O_3 pollution. The O_3 contribution of the residential and transportation
326 sources are less than $60 \mu\text{g m}^{-3}$ on average, further showing the important role of the industry
327 source in the O_3 pollution. When the industry and residential sources are not considered in
328 the simulation, the transportation source still causes the simulated $[O_3]$ to exceed $160 \mu\text{g m}^{-3}$,
329 particularly in NCPs. Taking into consideration the very fast increase of vehicles in China
330 recently (X. Wu et al., 2016), the transportation source increasingly constitutes a more
331 important O_3 source, particularly when the industry source is under control. Apparently,
332 when the industry and transportation sources are excluded or only residential source is
333 included, the high O_3 pollution is significantly mitigated and the simulated $[O_3]$ are less than
334 $160 \mu\text{g m}^{-3}$ on average. Figure 11 provides the distribution of the $[O_3]$ averaged during the
335 peak time on May 25 when the most serious O_3 pollution occurs during the simulated episode.
336 When only the industry emissions are considered, the O_3 pollution is mitigated considerably
337 in Eastern China, but still widespread in NCPs and PRDs. If only considering the



338 transportation source, the O₃ pollution still occurs in NCPs, with the [O₃] exceeding 160 µg
339 m⁻³. When the industry and transportation sources are excluded, the O₃ pollution is generally
340 under control. Hence, reducing the emissions from industry and transportation is a key to
341 mitigate O₃ pollution in Eastern China.

342

343 **4 Summary and Conclusions**

344 In the present study, air pollutants observations, released by China MEP, have been
345 analyzed to explore the O₃ pollution situation in Eastern China. Analysis of air pollutants
346 observations in 66 cities from 2013 to 2015 have shown that, although implementation of the
347 APPCAP has considerably decreased the CO, SO₂, NO₂, and PM_{2.5} mass concentrations from
348 April to September in Eastern China, the [O₃] have increased by 9.2% and the frequency of
349 O₃ exceedance with hourly [O₃] exceeding 200 µg m⁻³ has increased by about 25% in the
350 afternoon. Mitigation of NO_x and PM_{2.5} due to implementation of the APPCAP, increasing
351 transportation activities, or variability of meteorological situations perhaps contributes to the
352 deterioration of the O₃ pollution in Eastern China.

353 O₃ observations from April to September in 2015 have shown that Eastern China has
354 experienced widespread and persistent O₃ pollution. Only two cities in Eastern China have
355 observed the maximum 1-h [O₃] less than 200 µg m⁻³. Over 25% of cities have observed the
356 maximum 1-h [O₃] exceeding 400 µg m⁻³, particularly more than 800 µg m⁻³ [O₃] have been
357 observed in six cities in Eastern China. The average daily maximum 1-h [O₃] from April to
358 September exceed 160 µg m⁻³ in 45% of cities in Eastern China, and the 1-h [O₃] of 200 µg
359 m⁻³ have been exceeded on over 10% of days from April to September in 129 cities, and on
360 40% of days in 10 cities.

361 A widespread and severe O₃ pollution episode from 22 to 28 May 2015 in Eastern
362 China has been simulated using the WRF-CHEM model. The model generally simulates



363 reasonably well the temporal variations and spatial distributions of near-surface $[O_3]$, but the
364 uncertainties of meteorological fields or emission inventories still cause model
365 overestimation or underestimation. The model performs reasonably in simulating NO_2 , but
366 the model biases are rather large during nighttime.

367 FSA is utilized to assess the O_3 contribution of biogenic and various anthropogenic
368 sources. Sensitivity studies have shown that the industry source plays the most important role
369 in the O_3 pollution formation. When the simulated $[O_3]$ are more than around $200 \mu g m^{-3}$, the
370 O_3 contribution from the industry emissions generally exceeds $50 \mu g m^{-3}$ in Eastern China,
371 particularly when the simulated $[O_3]$ exceed $300 \mu g m^{-3}$, the industrial O_3 contribution
372 constitutes one third of the $[O_3]$. The transportation emission is the second most important O_3
373 source in NEC, YRDs, and PRDs, but its O_3 contribution is much less than that from the
374 industry source when the simulated $[O_3]$ exceed $150 \mu g m^{-3}$. The biogenic source plays a
375 more important role in O_3 formation than the transportation source in PRDs, with the O_3
376 contribution exceeding $50 \mu g m^{-3}$ when simulated $[O_3]$ are more than $250 \mu g m^{-3}$. In general,
377 the O_3 contribution from residential source is not significant. Further sensitivity studies have
378 also indicated that if only considering the residential source or excluding the industry and
379 transportation sources in simulations, the O_3 pollution in Eastern China could be significantly
380 improved. Only the industry or transportation source still causes O_3 pollution, particularly
381 with regard to the industry source.

382 Widespread and persistent O_3 pollution poses adverse impacts on ecosystems and
383 human health. Considering the key role of the industry source in the high O_3 formation,
384 mitigation of the industry source becomes the top choice to improve the O_3 pollution in
385 Eastern China, particularly with regard to the VOCs emissions that are still not fully
386 considered in the current air pollutant control strategy. Rapid increase of vehicles also
387 enhances the VOCs and NO_x emissions and the transportation source plays an increasingly



388 important role in the O₃ pollution. In addition, the rapid decrease of PM_{2.5} due to
389 implementation of the APPCAP reduces the aerosol and cloud optical depth, which is subject
390 to enhance the O₃ formation by increasing the photolysis. Hence, stringent control strategies
391 of VOCs and NO_x need to be designed comprehensively and implemented to avoid the
392 looming severe O₃ pollution in Eastern China.

393 Although the model performs generally well in simulating O₃ and NO₂ during a seven-
394 day O₃ pollution episode in Eastern China, uncertainties from meteorological fields
395 simulations and emissions inventory still cause model biases. Taking into consideration the
396 complexity of the O₃ formation and rapid changes of emissions inventories, further model
397 studies need to be performed to investigate the O₃ formation for supporting the design and
398 implementation of emission control strategies, based on the improved meteorological fields
399 simulations.

400

401 *Acknowledgements.* This work was supported by the National Natural Science Foundation of
402 China (No. 41275153) and by the "Strategic Priority Research Program" of the Chinese
403 Academy of Sciences, Grant No. XDB05060500. Guohui Li is also supported by the
404 "Hundred Talents Program" of the Chinese Academy of Sciences. Naifang Bei is supported
405 by the National Natural Science Foundation of China (No. 41275101). Wenting Dai is
406 supported by the National Natural Science Foundation of China (No. 41503117).

407

408 **Reference**

- 409 Banta, R. M., Senff, C. J., Nielsen-Gammon, J., Darby, L. S., Ryerson, T. B., Alvarez, R. J.,
410 Sandberg, S. R., Williams, E. J., and Trainer, M.: A bad air day in Houston, *Bull. Amer.*
411 *Meteorol. Soc.*, 86, 657-669, 10.1175/bams-86-5-657, 2005.
- 412 Bei, N., Lei, W., Zavala, M., and Molina, L. T.: Ozone predictabilities due to meteorological
413 uncertainties in the Mexico City basin using ensemble forecasts, *Atmos. Chem. Phys.*, 10,
414 6295-6309, 10.5194/acp-10-6295-2010, 2010.
- 415 Bei, N., Li, G., and Molina, L. T.: Uncertainties in SOA simulations due to meteorological
416 uncertainties in Mexico City during MILAGRO-2006 field campaign, *Atmos. Chem.*
417 *Phys.*, 12, 11295-11308, 10.5194/acp-12-11295-2012, 2012.
- 418 Bell, M. L., Peng, R. D., and Dominici, F.: The exposure-response curve for ozone and risk
419 of mortality and the adequacy of current ozone regulations, *Environ. Health Persp.*, 114,
420 532-536, 10.1289/ehp.8816, 2006.
- 421 Binkowski, F. S., and Roselle, S. J.: Models-3 community multiscale air quality (CMAQ)
422 model aerosol component - I. Model description, *J. Geophys. Res.*, 108, 18,
423 10.1029/2001jd001409, 2003.
- 424 Brasseur, G. P., Orlando, J. J., and Tyndall, G. S.: Atmospheric chemistry and global change,
425 Oxford University Press, Cambridge, USA, 654 pp., 1999.
- 426 Cao, J. J., Xu, H. M., Xu, Q., Chen, B. H., and Kan, H. D.: Fine Particulate Matter
427 Constituents and Cardiopulmonary Mortality in a Heavily Polluted Chinese City, *Environ.*
428 *Health Persp.*, 120, 373-378, 10.1289/ehp.1103671, 2012.
- 429 Chameides, W. L., Lindsay, R. W., Richardson, J., and Kiang, C. S.: The role of biogenic
430 hydrocarbons in urban photochemical smog - Atlanta as a case-study, *Science*, 241, 1473-
431 1475, 10.1126/science.3420404, 1988.
- 432 Chen, F., and Dudhia, J.: Coupling an advanced land surface-hydrology model with the Penn
433 State-NCAR MM5 modeling system. Part I: Model implementation and sensitivity, *Mon.*
434 *Weather Rev.*, 129, 569-585, 10.1175/1520-0493(2001)129<0569:caalsh>2.0.co;2, 2001.
- 435 Chen, W., Yan, L., and Zhao, H. M.: Seasonal Variations of Atmospheric Pollution and Air
436 Quality in Beijing, *Atmosphere*, 6, 1753-1770, 10.3390/atmos6111753, 2015.
- 437 Cheng, N., Li, Y., Zhang, D., Chen, T., Sun, F., Chen, C., and Meng, F.: Characteristics of
438 Ground Ozone Concentration over Beijing from 2004 to 2015: Trends, Transport, and
439 Effects of Reductions, *Atmos. Chem. Phys. Discuss.*, 2016, 1-21, 10.5194/acp-2016-508,
440 2016.
- 441 Chou, M.-D. and M. J. Suarez: A solar radiation parameterization for atmospheric studies,
442 NASA Tech. Rep. NASA/TM-1999-10460, 15, 38 pp, 1999.
- 443 Chou, M.-D. and M. J. Suarez: A thermal infrared radiation parameterization for atmospheric
444 studies, NASA/TM-2001-104606, 19, 55 pp, 2001.
- 445 Feng, T., Bei, N., Huang, R. J., Cao, J., Zhang, Q., Zhou, W., Tie, X., Liu, S., Zhang, T., Su,
446 X., Lei, W., Molina, L. T., and Li, G.: Summertime ozone formation in Xi'an and
447 surrounding areas, China, *Atmos. Chem. Phys.*, 16, 4323-4342, 10.5194/acp-16-4323-
448 2016, 2016.



- 449 Grell, G. A., Peckham, S. E., Schmitz, R., McKeen, S. A., Frost, G., Skamarock, W. C., and
450 Eder, B.: Fully coupled “online” chemistry within the WRF model, *Atmos. Environ.*, 39,
451 6957-6975, 10.1016/j.atmosenv.2005.04.027, 2005.
- 452 Guenther, A., Karl, T., Harley, P., Wiedinmyer, C., Palmer, P. I., and Geron, C.: Estimates of
453 global terrestrial isoprene emissions using MEGAN (Model of Emissions of Gases and
454 Aerosols from Nature), *Atmos. Chem. Phys.*, 6, 3181-3210, 2006.
- 455 Huang, M., Carmichael, G. R., Spak, S. N., Adhikary, B., Kulkarni, S., Cheng, Y., Wei, C.,
456 Tang, Y., D’Allura, A., Wennberg, P. O., Huey, G. L., Dibb, J. E., Jimenez, J. L., Cubison,
457 M. J., Weinheimer, A. J., Kaduwela, A., Cai, C., Wong, M., Pierce, R. B., Al-Saadi, J. A.,
458 Streets, D. G., and Zhang, Q.: Multi-scale modeling study of the source contributions to
459 near-surface ozone and sulfur oxides levels over California during the ARCTAS-CARB
460 period, *Atmos. Chem. Phys.*, 11, 3173-3194, 10.5194/acp-11-3173-2011, 2011.
- 461 Hong, S.-Y., and Lim, J.-O. J.: The WRF Single-Moment 6-Class Microphysics Scheme
462 (WSM6), *Asia-Pacific Journal of Atmospheric Sciences*, 42, 129-151, 2006.
- 463 Horowitz, L. W., Walters, S., Mauzerall, D. L., Emmons, L. K., Rasch, P. J., Granier, C., Tie,
464 X. X., Lamarque, J. F., Schultz, M. G., Tyndall, G. S., Orlando, J. J., and Brasseur, G. P.:
465 A global simulation of tropospheric ozone and related tracers: Description and evaluation
466 of MOZART, version 2, *J. Geophys. Res.*, 108, 29, 10.1029/2002jd002853, 2003.
- 467 Janjić, Z. I.: Nonsingular Implementation of the Mellor–Yamada Level 2.5 Scheme in the
468 NCEP Meso Model, *Ncep Office Note*, 436, 2002.
- 469 Kurokawa, J., Ohara, T., Morikawa, T., Hanayama, S., Janssens-Maenhout, G., Fukui, T.,
470 Kawashima, K., and Akimoto, H.: Emissions of air pollutants and greenhouse gases over
471 Asian regions during 2000-2008: Regional Emission inventory in ASia (REAS) version 2,
472 *Atmos. Chem. Phys.*, 13, 11019-11058, 10.5194/acp-13-11019-2013, 2013.
- 473 Li, G., Zhang, R., Fan, J., and Tie, X.: Impacts of black carbon aerosol on photolysis and
474 ozone, *J. Geophys. Res.*, 110, 10.1029/2005jd005898, 2005.
- 475 Li, G., Zhang, R., Fan, J., and Tie, X.: Impacts of biogenic emissions on photochemical
476 ozone production in Houston, Texas, *J. Geophys. Res.*, 112, 10.1029/2006jd007924, 2007.
- 477 Li, G., Lei, W., Zavala, M., Volkamer, R., Dusanter, S., Stevens, P., and Molina, L. T.:
478 Impacts of HONO sources on the photochemistry in Mexico City during the MCMA-
479 2006/MILAGO Campaign, *Atmos. Chem. Phys.*, 10, 6551-6567, 10.5194/acp-10-6551-
480 2010, 2010.
- 481 Li, G., Bei, N., Tie, X., and Molina, L. T.: Aerosol effects on the photochemistry in Mexico
482 City during MCMA-2006/MILAGRO campaign, *Atmos. Chem. Phys.*, 11, 5169-5182,
483 10.5194/acp-11-5169-2011, 2011a.
- 484 Li, G., Zavala, M., Lei, W., Tsimpidi, A. P., Karydis, V. A., Pandis, S. N., Canagaratna, M.
485 R., and Molina, L. T.: Simulations of organic aerosol concentrations in Mexico City using
486 the WRF-CHEM model during the MCMA-2006/MILAGRO campaign, *Atmos. Chem.*
487 *Phys.*, 11, 3789-3809, 10.5194/acp-11-3789-2011, 2011b.
- 488 Li, G., Lei, W., Bei, N., and Molina, L. T.: Contribution of garbage burning to chloride and
489 PM_{2.5} in Mexico City, *Atmos. Chem. Phys.*, 12, 8751-8761, 10.5194/acp-12-8751-2012,
490 2012.



- 491 Li, G. H., Bei, N. F., Zavala, M., and Molina, L. T.: Ozone formation along the California
492 Mexican border region during Cal-Mex 2010 field campaign, *Atmos. Environ.*, 88, 370-
493 389, 10.1016/j.atmosenv.2013.11.067, 2014.
- 494 Lippmann, M.: Health-effects of tropospheric ozone - review of recent research findings and
495 their implications to ambient air-quality standards, *J. Expo. Anal. Environ. Epidemiol.*, 3,
496 103-129, 1993.
- 497 Ma, Z. Q., Xu, J., Quan, W. J., Zhang, Z. Y., Lin, W. L., and Xu, X. B.: Significant increase
498 of surface ozone at a rural site, north of eastern China, *Atmos. Chem. Phys.*, 16, 3969-
499 3977, 2016.
- 500 National Research Council (1991), *Rethinking the Ozone Problem in Urban and Regional Air*
501 *Pollution*, National Academy Press, Washington, D.C.
- 502 Nenes, A., Pandis, S. N., and Pilinis, C.: ISORROPIA: A new thermodynamic equilibrium
503 model for multiphase multicomponent inorganic aerosols, *Aquat. Geochem.*, 4, 123-152,
504 10.1023/a:1009604003981, 1998.
- 505 Ou, J. M., Yuan, Z. B., Zheng, J. Y., Huang, Z. J., Shao, M., Li, Z. K., Huang, X. B., Guo, H.,
506 and Louie, P. K. K.: Ambient Ozone Control in a Photochemically Active Region: Short
507 Term Despiking or Long-Term Attainment?, *Environ. Sci. Technol.*, 50, 5720-5728,
508 10.1021/acs.est.6b00345, 2016.
- 509 Richter, A., Burrows, J. P., Nuss, H., Granier, C., and Niemeier, U.: Increase in tropospheric
510 nitrogen dioxide over China observed from space, *Nature*, 437, 129-132,
511 10.1038/nature04092, 2005.
- 512 Tao, Z. N., Larson, S. M., Wuebbles, D. J., Williams, A., and Caughey, M.: A summer
513 simulation of biogenic contributions to ground-level ozone over the continental United
514 States, *J. Geophys. Res.*, 108, 24, 10.1029/2002jd002945, 2003.
- 515 Tie, X., Geng, F., Guenther, A., Cao, J., Greenberg, J., Zhang, R., Apel, E., Li, G.,
516 Weinheimer, A., Chen, J., and Cai, C.: Megacity impacts on regional ozone formation:
517 observations and WRF-Chem modeling for the MIRAGE-Shanghai field campaign,
518 *Atmos. Chem. Phys.*, 13, 5655-5669, 10.5194/acp-13-5655-2013, 2013.
- 519 Tie, X. X., Madronich, S., Walters, S., Zhang, R. Y., Rasch, P., and Collins, W.: Effect of
520 clouds on photolysis and oxidants in the troposphere, *J. Geophys. Res.*, 108, 25,
521 10.1029/2003jd003659, 2003.
- 522 Wang, S. W., Zhang, Q., Streets, D. G., He, K. B., Martin, R. V., Lamsal, L. N., Chen, D.,
523 Lei, Y., and Lu, Z.: Growth in NO_x emissions from power plants in China: bottom-up
524 estimates and satellite observations, *Atmos. Chem. Phys.*, 12, 4429-4447, 10.5194/acp-
525 12-4429-2012, 2012.
- 526 Wang, T., Ding, A. J., Gao, J., and Wu, W. S.: Strong ozone production in urban plumes
527 from Beijing, China, *Geophys. Res. Lett.*, 33, 5, 10.1029/2006gl027689, 2006.
- 528 Wang, Y., Zhang, Q. Q., He, K., Zhang, Q., and Chai, L.: Sulfate-nitrate-ammonium aerosols
529 over China: response to 2000-2015 emission changes of sulfur dioxide, nitrogen oxides,
530 and ammonia, *Atmos. Chem. Phys.*, 13, 2635-2652, 10.5194/acp-13-2635-2013, 2013.
- 531 Wang, Z., Zeng, H., Wei, Y., and Zhang, Y.: Regional total factor energy efficiency: An
532 empirical analysis of industrial sector in China, *Appl. Energ.*, 2012, 97, 115-123, 2012.
- 533 Weinhold, B.: Ozone nation - EPA standard panned by the people, *Environ. Health Persp.*,
534 116, A302-A305, 2008.



- 535 Wesely, M. L.: Parameterization of surface resistances to gaseous dry deposition in regional-
536 scale numerical models, *Atmos. Environ.*, 23, 1293-1304, [http://dx.doi.org/10.1016/0004-](http://dx.doi.org/10.1016/0004-6981(89)90153-4)
537 6981(89)90153-4, 1989.
- 538 Wu, J., Li, G., Cao, J., Bei, N., Wang, Y., Feng, T., Huang, R., Liu, S., Zhang, Q., and Tie, X.:
539 Contributions of Trans-boundary Transport to the Summertime Air Quality in Beijing,
540 China, *Atmos. Chem. Phys. Discuss.*, 2016, 1-46, 10.5194/acp-2016-705, 2016.
- 541 Wu, X., Wu, Y., Zhang, S., Liu, H., Fu, L., and Hao, J.: Assessment of vehicle emission
542 programs in China during 1998-2013: Achievement, challenges and implications,
543 *Environ. Pollut.*, 2016, 214, 556-567, 2016.
- 544 Xing, J., Wang, S. X., Chatani, S., Zhang, C. Y., Wei, W., Hao, J. M., Klimont, Z., Cofala, J.,
545 and Amann, M.: Projections of air pollutant emissions and its impacts on regional air
546 quality in China in 2020, *Atmos. Chem. Phys.*, 11, 3119-3136, 10.5194/acp-11-3119-
547 2011, 2011.
- 548 Xu J, Ma J Z, Zhang X L, et al. Measurements of ozone and its precursors in Beijing during
549 summertime: impact of urban plumes on ozone pollution in downwind rural areas, *Atmos.*
550 *Chem. Phys.*, 2011, 11, 12241-12252.
- 551 Yang, X. F., Liu, H., Man, H. Y., and He, K. B.: Characterization of road freight
552 transportation and its impact on the national emission inventory in China, *Atmos. Chem.*
553 *Phys.*, 15, 2105-2118, doi:10.5194/acp-15-2105-2015, 2015.
- 554 Zhang, Q., Streets, D. G., Carmichael, G. R., He, K. B., Huo, H., Kannari, A., Klimont, Z.,
555 Park, I. S., Reddy, S., Fu, J. S., Chen, D., Duan, L., Lei, Y., Wang, L. T., and Yao, Z. L.:
556 Asian emissions in 2006 for the NASA INTEX-B mission, *Atmos. Chem. Phys.*, 9, 5131-
557 5153, doi:10.5194/acp-9-5131-2009, 2009.
- 558 Zhou, J. A., Ito, K., Lall, R., Lippmann, M., and Thurston, G.: Time-Series Analysis of
559 Mortality Effects of Fine Particulate Matter Components in Detroit and Seattle, *Environ.*
560 *Health Persp.*, 119, 461-466, 10.1289/ehp.1002613, 2011.
- 561
562



563 Table 1 WRF-CHEM model configurations

564

Regions	Eastern China
Simulation period	May 22 to 28, 2015
Domain size	350 × 350
Domain center	35°N, 114°E
Horizontal resolution	10km × 10km
Vertical resolution	35 vertical levels with a stretched vertical grid with spacing ranging from 30 m near the surface, to 500 m at 2.5 km and 1 km above 14 km
Microphysics scheme	WSM 6-class graupel scheme (Hong and Lim, 2006)
Boundary layer scheme	MYJ TKE scheme (Janjić, 2002)
Surface layer scheme	MYJ surface scheme (Janjić, 2002)
Land-surface scheme	Unified Noah land-surface model (Chen and Dudhia, 2001)
Longwave radiation scheme	Goddard longwave scheme (Chou and Suarez, 2001)
Shortwave radiation scheme	Goddard shortwave scheme (Chou and Suarez, 1999)
Meteorological boundary and initial conditions	NCEP 1°×1° reanalysis data
Chemical initial and boundary conditions	MOZART 6-hour output (Horowitz et al., 2003)
Anthropogenic emission inventory	SAPRC-99 chemical mechanism emissions (Zhang et al., 2009)
Biogenic emission inventory	MEGAN model developed by Guenther et al. (2006)
Model spin-up time	28 hours

565

566



567 Table 2 Observed hourly mass concentrations of pollutants averaged in the afternoon from
568 April to September 2013 and 2015 in 65 cities of Eastern China.
569

Pollutants	CO (mg m^{-3})	SO ₂ ($\mu\text{g m}^{-3}$)	NO ₂ ($\mu\text{g m}^{-3}$)	O ₃ ($\mu\text{g m}^{-3}$)	PM _{2.5} ($\mu\text{g m}^{-3}$)
2013	1.05	24.8	27.7	100.5	46.9
2015	0.77	15.4	23.9	110.5	38.2
Change (%)	-26.7	-37.8	-13.5	+9.9	-18.5

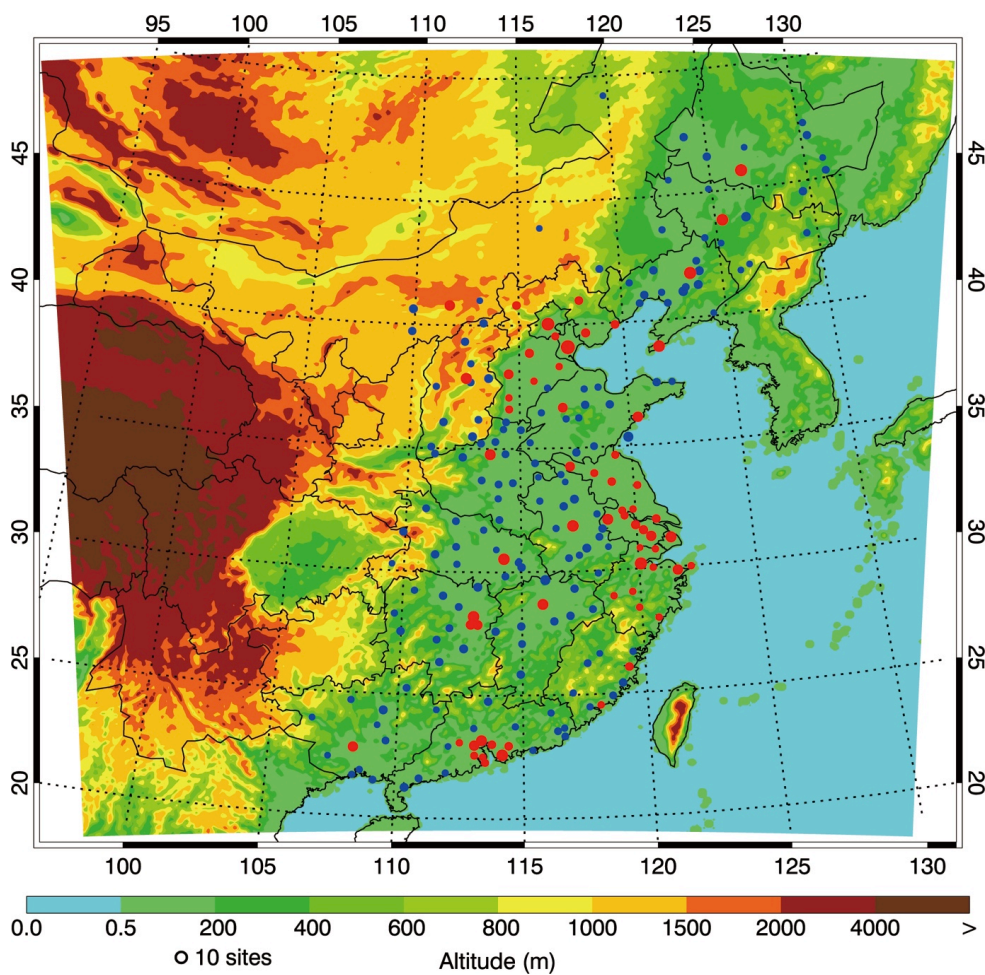
570

571



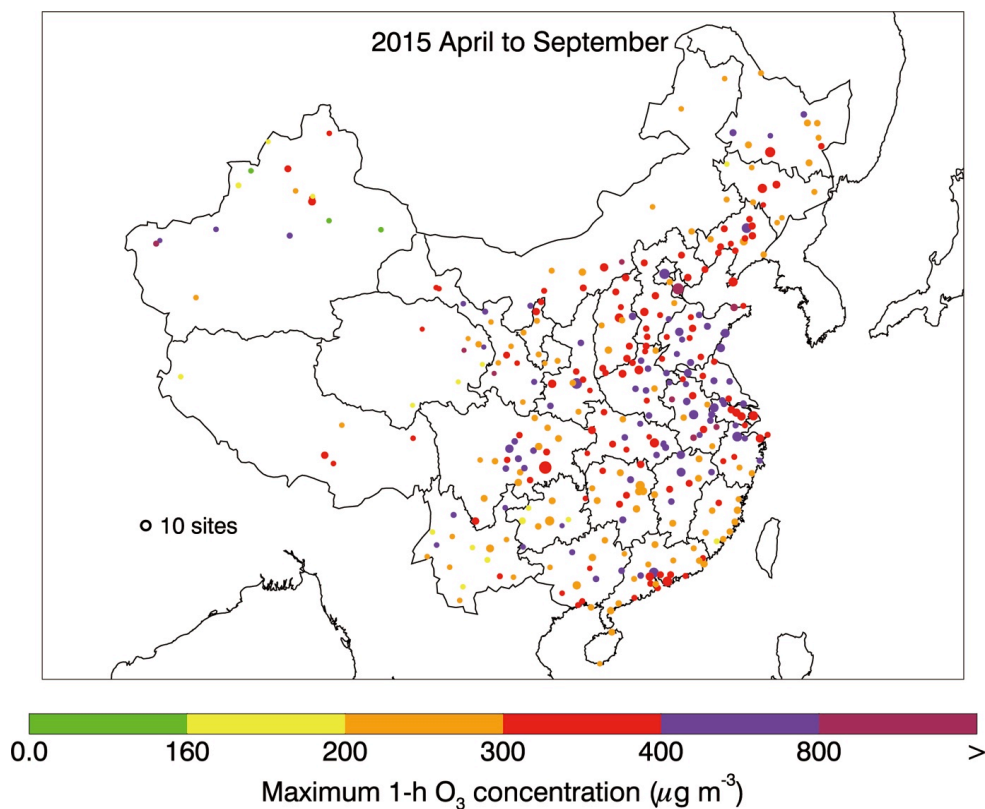
Figure Captions

- 572
573
574 Figure 1 WRF-CHEM simulation domain with topography. The filled circles represent
575 centers of cities with ambient monitoring sites and the size of circles denotes the
576 number of ambient monitoring sites of cities. The red and blue filled circles show
577 the cities with air pollutants observations since 2013 and 2015, respectively.
578
579 Figure 2 Distribution of observed maximum 1-h [O₃] in Mainland China from April to
580 September 2015.
581
582 Figure 3 Distribution of average daily maximum 1-h [O₃] in Mainland China from April to
583 September 2015.
584
585 Figure 4 Distribution of days with the maximum 1-h [O₃] exceeding 160 µg m⁻³ in Mainland
586 China from April to September 2015.
587
588 Figure 5 Distribution of days with the maximum 1-h [O₃] exceeding 200 µg m⁻³ in Mainland
589 China from April to September 2015.
590
591 Figure 6 Pattern comparison of simulated vs. observed near-surface O₃ at 15:00 BJT from 22
592 to 27 May 2015. Colored circles: O₃ observations; color contour: O₃ simulations;
593 black arrows: simulated surface winds.
594
595 Figure 7 Comparison of measured (black dots) and predicted (blue line) diurnal profiles of
596 near-surface O₃ averaged over all ambient monitoring stations in provinces of
597 Eastern China from 22 to 28 May 2015.
598
599 Figure 8 Distributions of the contribution to near-surface [O₃] averaged in the afternoon
600 during the whole episode from (a) industry, (b) residential, (c) transportation, and
601 (d) biogenic emissions.
602
603 Figure 9 O₃ contributions of industry (red line), residential (brown line), transportation (blue
604 line), and biogenic emissions (green line) in NEC, NCPs, YRDs, and PRDs, as a
605 function of simulated [O₃] in the control case.
606
607 Figure 10 O₃ contributions of industry alone (red line), residential (brown line), and
608 transportation emissions (blue line) in NEC, NCPs, YRDs, and PRDs, as a function
609 of simulated [O₃] in the control case.
610
611 Figure 11 Distributions of the average O₃ concentration during peak time with (a) all
612 anthropogenic emissions, (b) industry emissions alone, (c) residential emissions
613 alone, and (d) transportation emissions alone on May 2015.
614



615
616
617
618
619
620
621

Figure 1 WRF-CHEM simulation domain with topography. The filled circles represent centers of cities with ambient monitoring sites and the size of circles denotes the number of ambient monitoring sites of cities. The red and blue filled circles show the cities with air pollutants observations since 2013 and 2015, respectively.



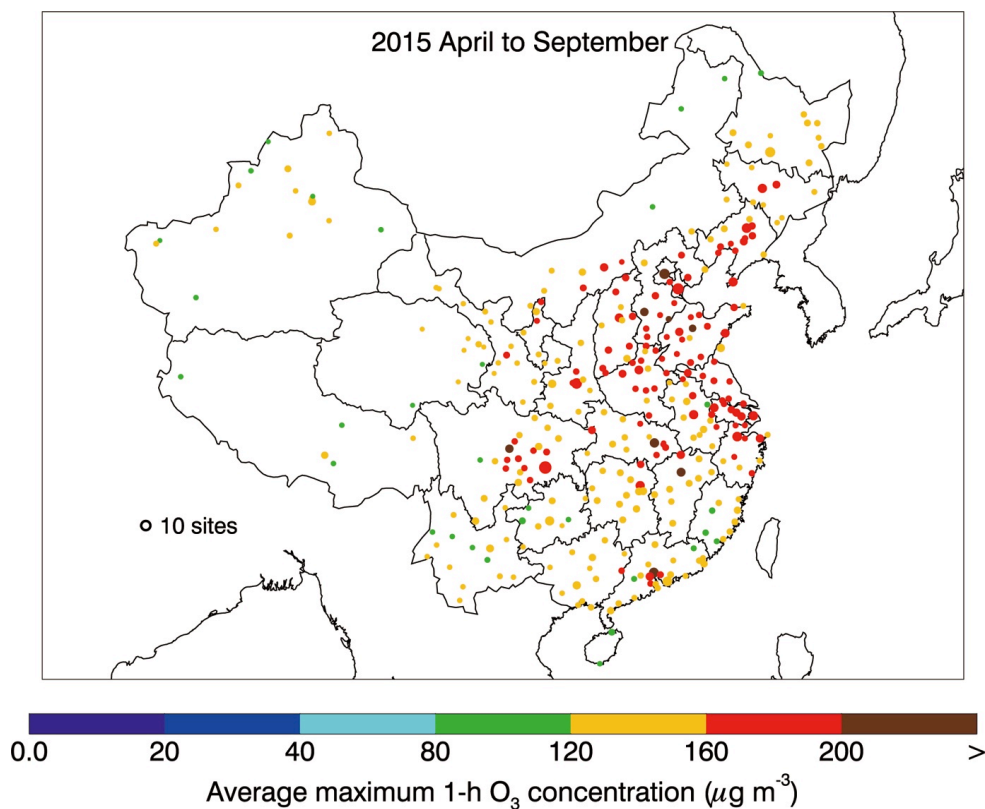
622

623

624 Figure 2 Distribution of observed maximum 1-h [O₃] in Mainland China from April to

625 September 2015.

626



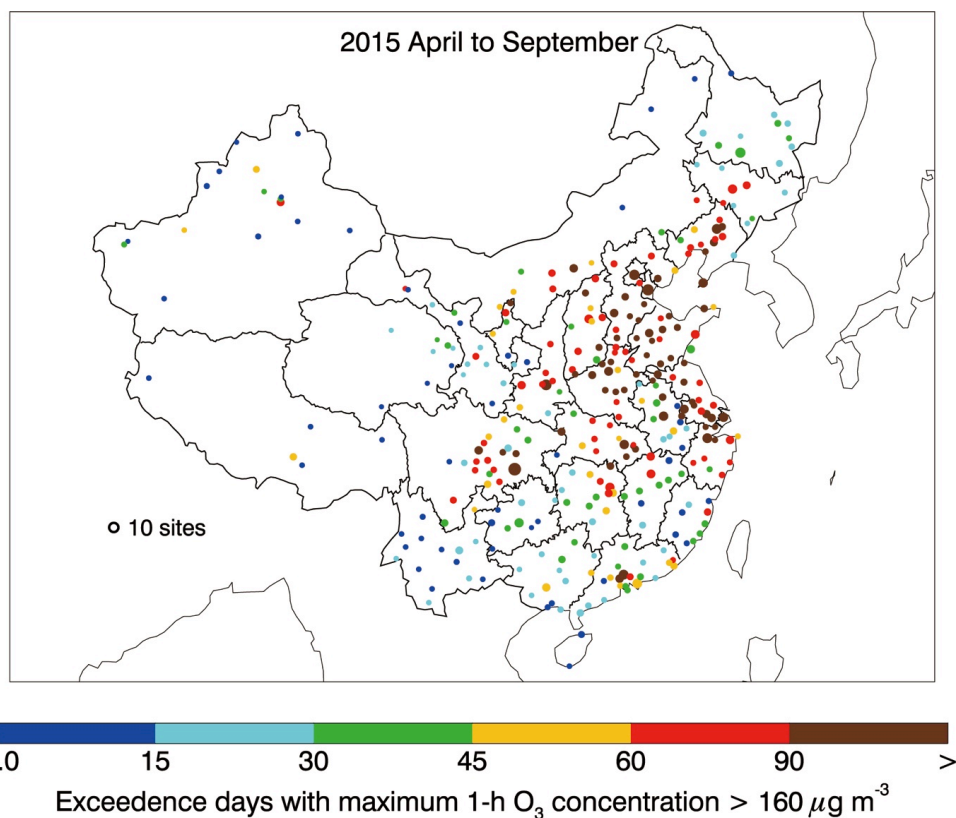
627

628

629 Figure 3 Distribution of average daily maximum 1-h $[O_3]$ in Mainland China from April to

630 September 2015.

631



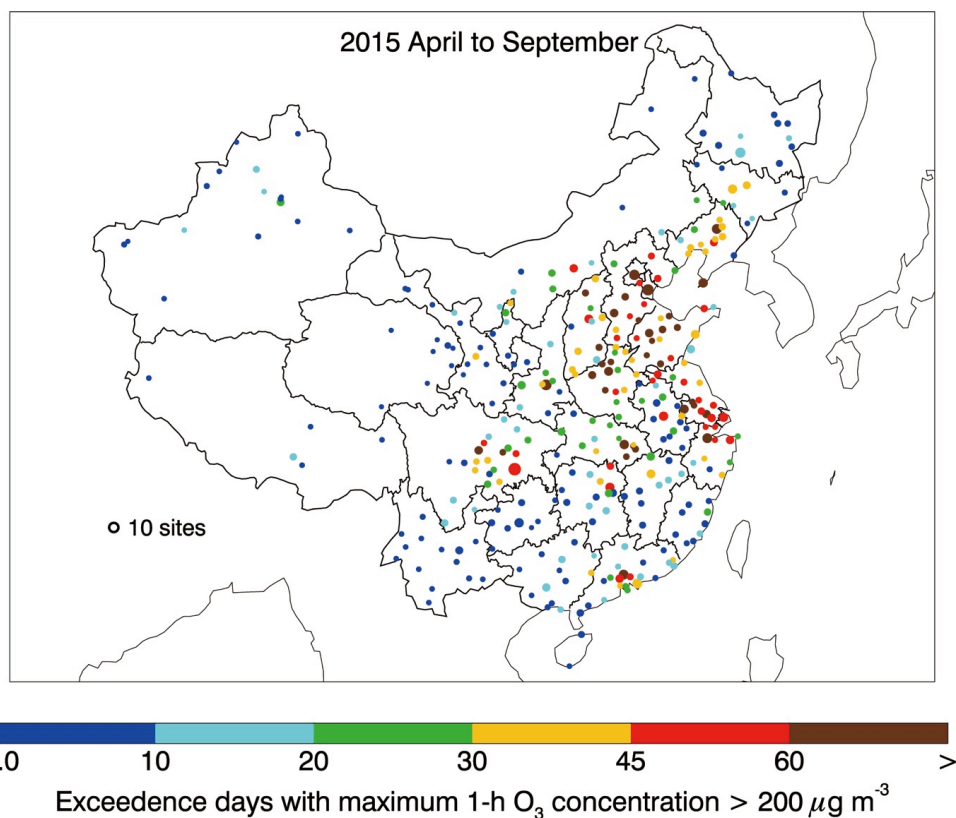
632

633

634 Figure 4 Distribution of days with the maximum 1-h $[O_3]$ exceeding $160 \mu g m^{-3}$ in Mainland

635 China from April to September 2015.

636



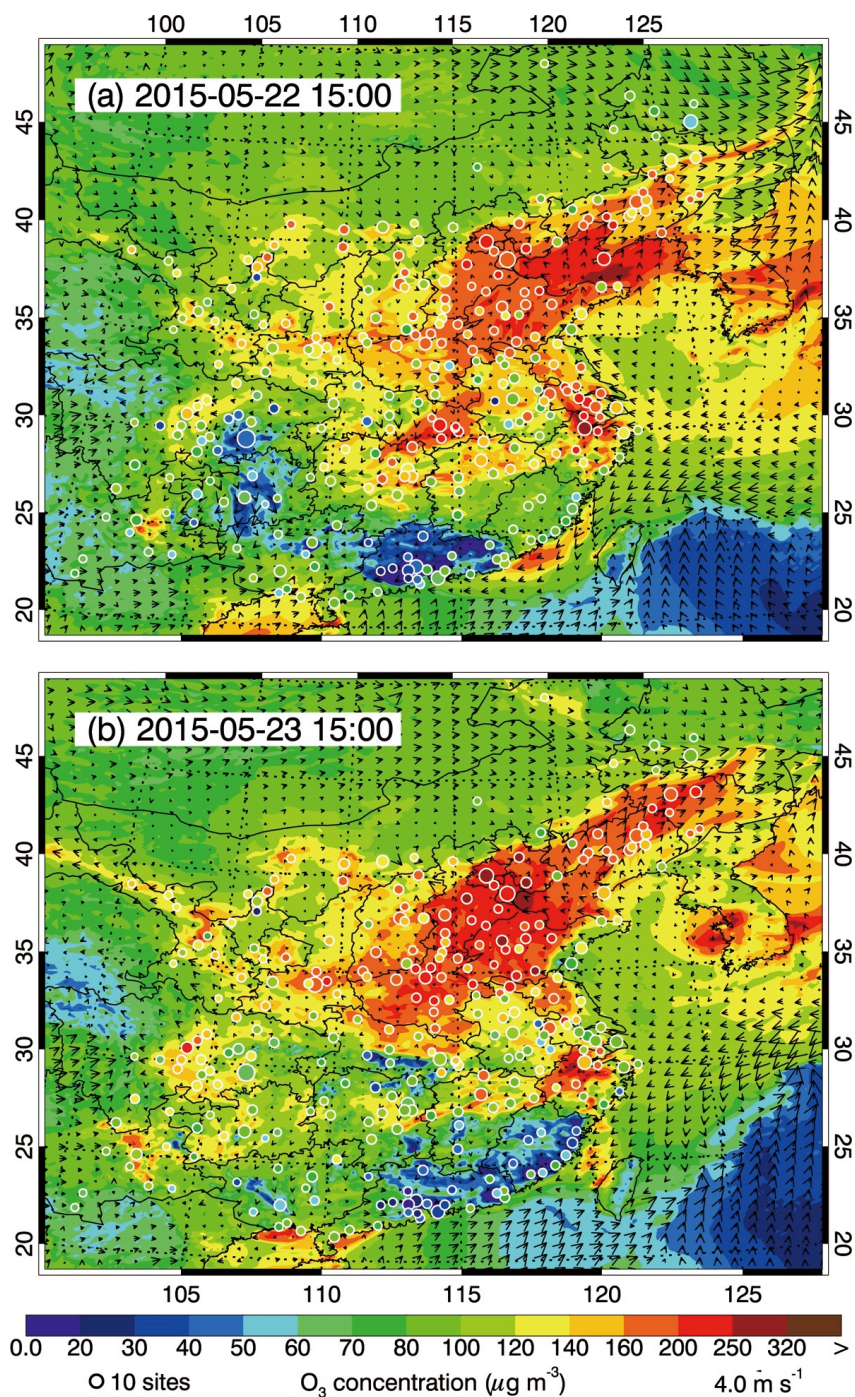
637

638

639 Figure 5 Distribution of days with the maximum 1-h $[O_3]$ exceeding $200 \mu g m^{-3}$ in Mainland

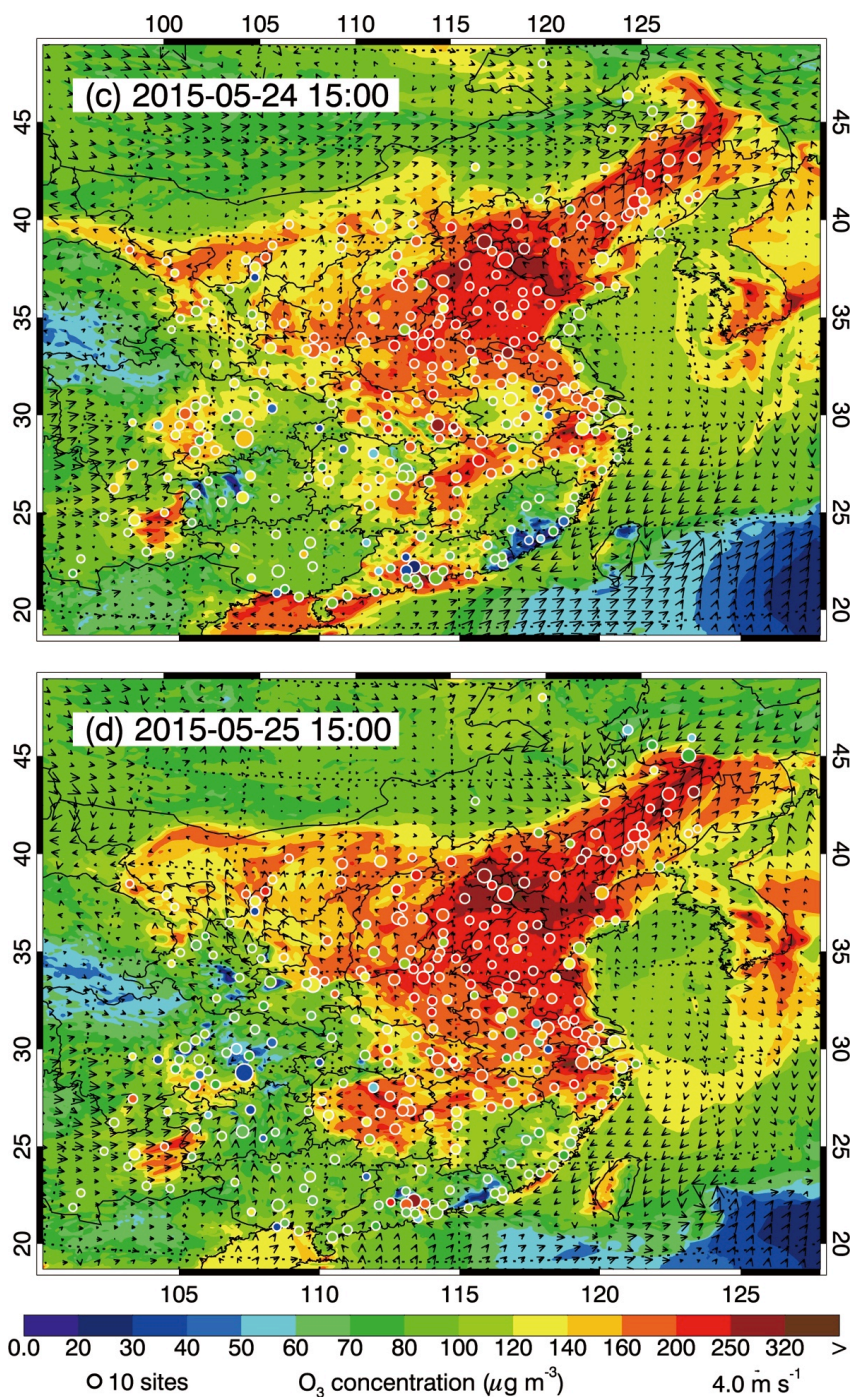
640 China from April to September 2015.

641



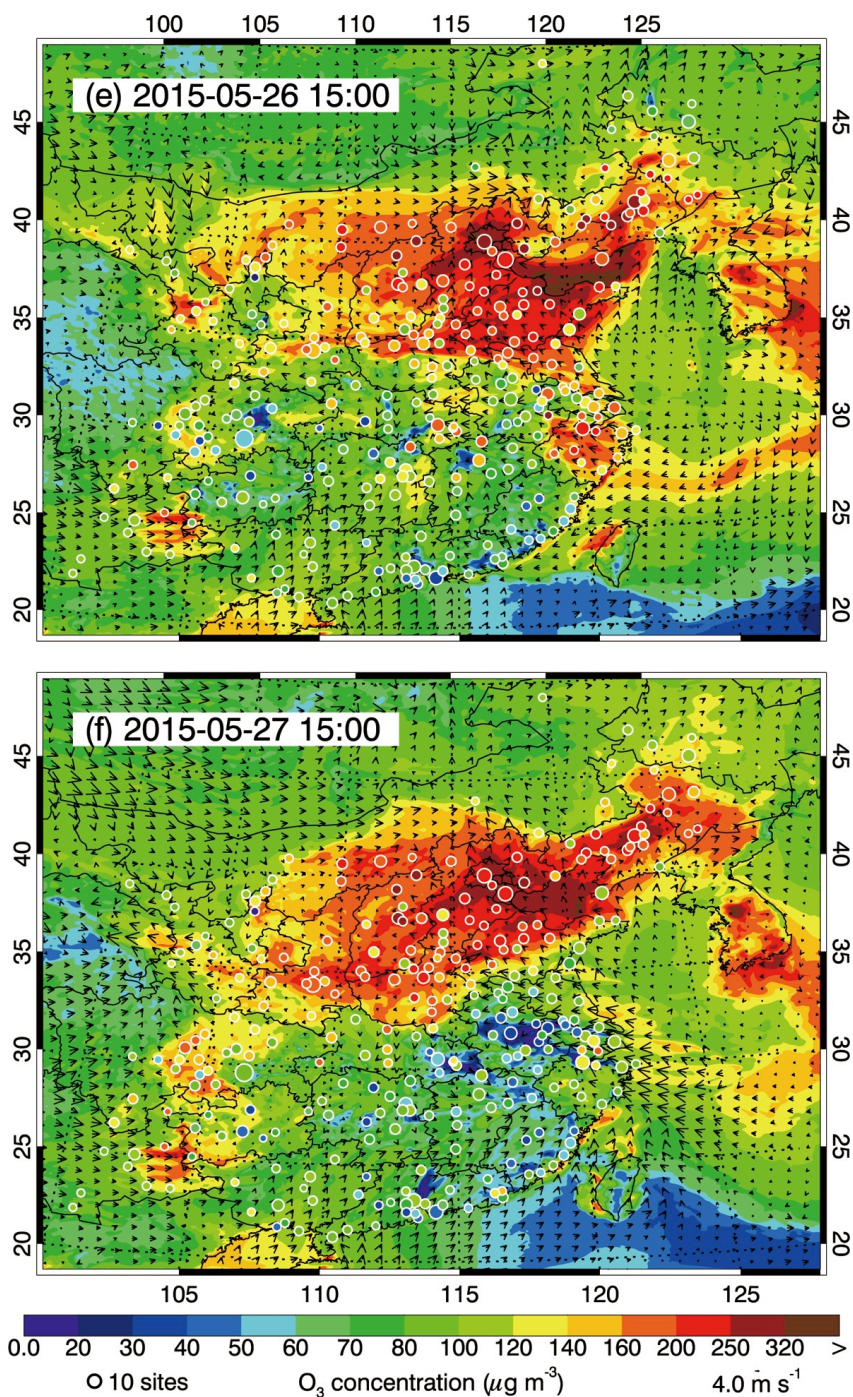
642
643
644
645
646

Figure 6 Pattern comparison of simulated vs. observed near-surface O₃ at 15:00 BJT from 22 to 27 May 2015. Colored circles: O₃ observations; color contour: O₃ simulations; black arrows: simulated surface winds.



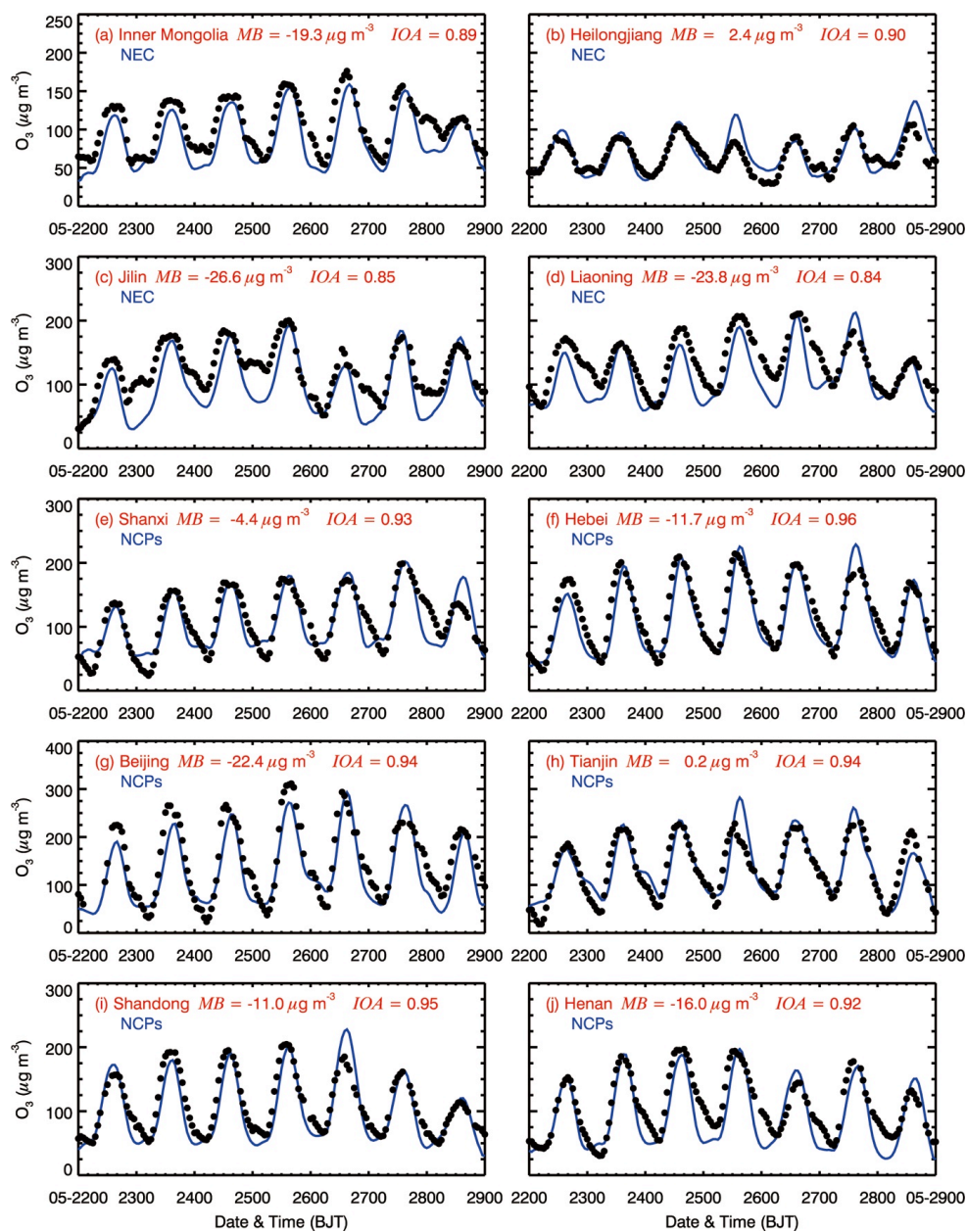
647
648
649
650

Figure 6 continued



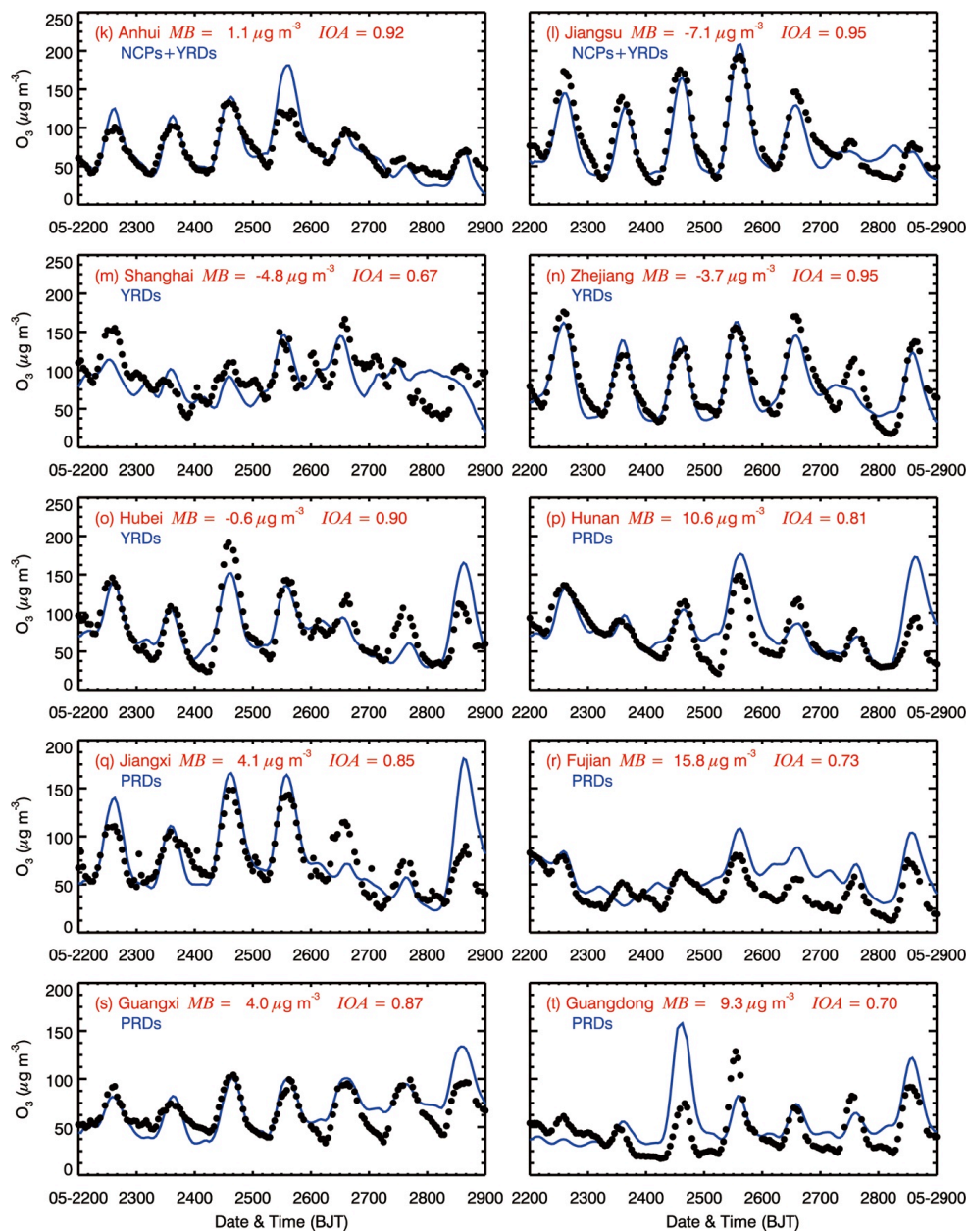
651
652
653
654

Figure 6 continued



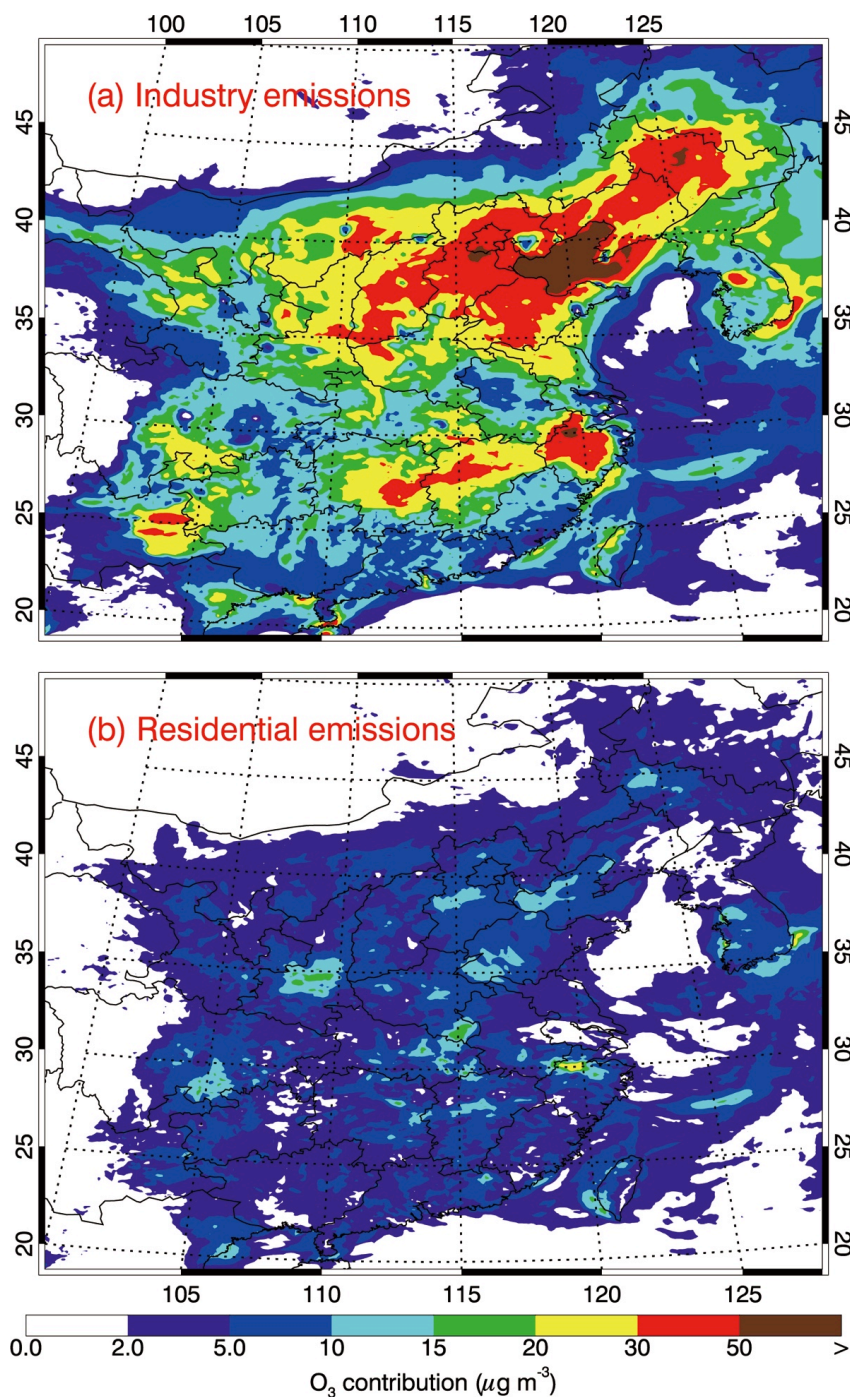
655
656
657
658
659
660

Figure 7 Comparison of measured (black dots) and predicted (blue line) diurnal profiles of near-surface O_3 averaged over all ambient monitoring stations in provinces of Eastern China from 22 to 28 May 2015.



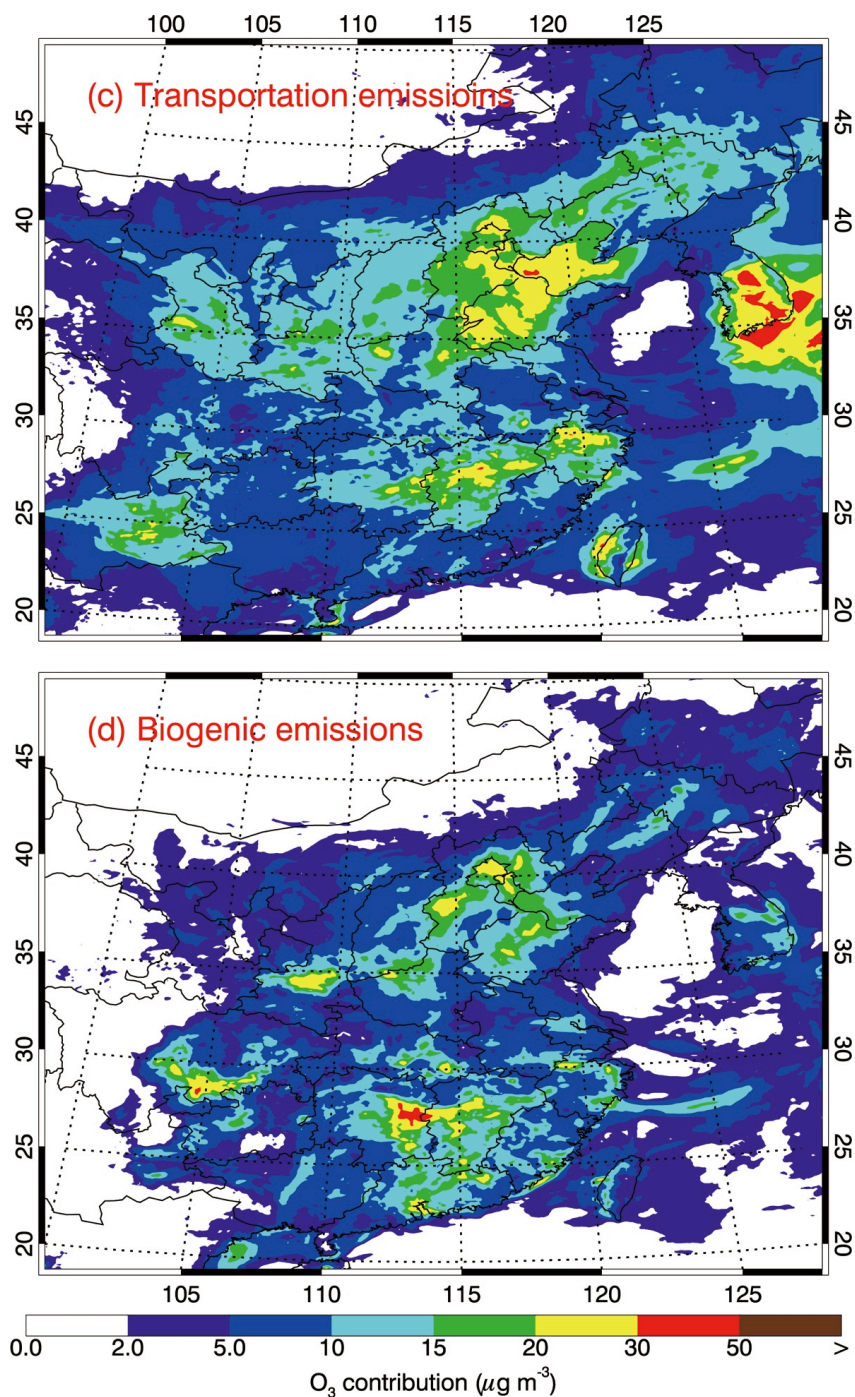
661
 662
 663
 664

Figure 7 continued



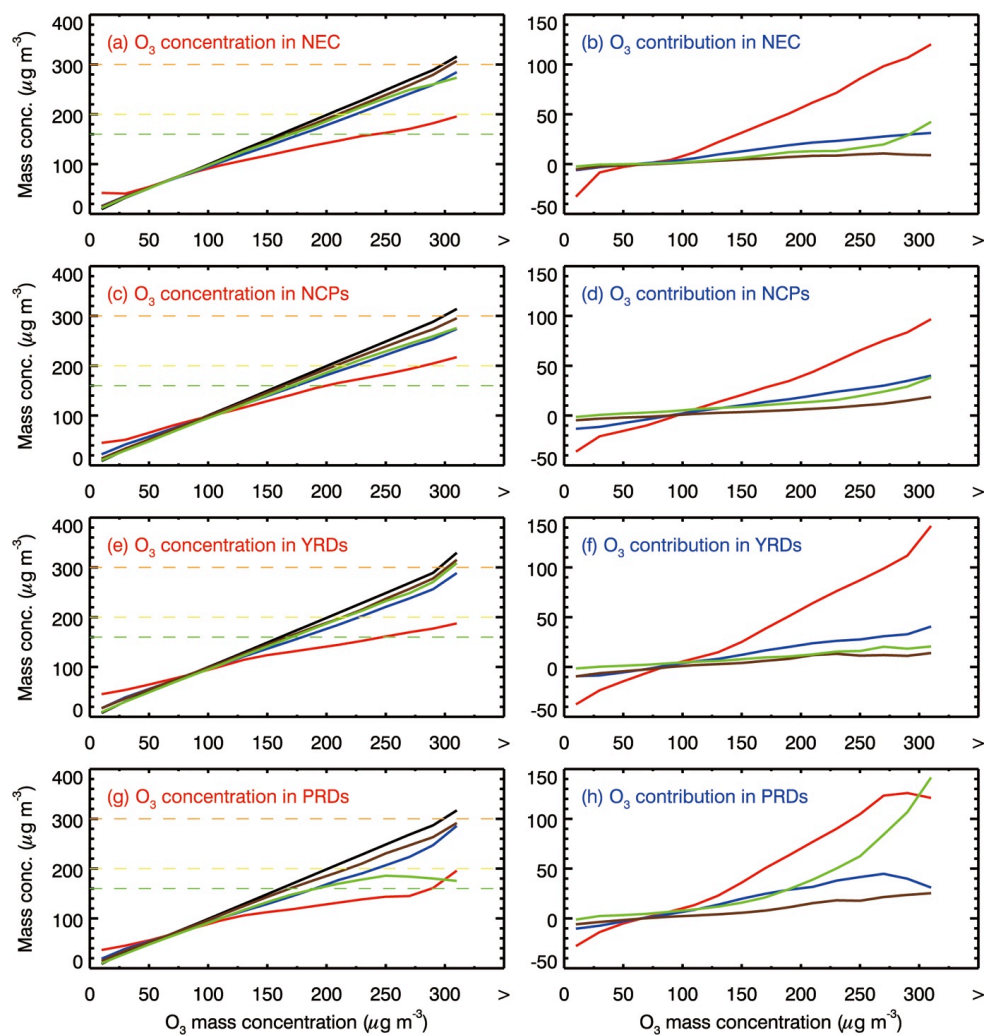
665
666
667
668
669

Figure 8 Distributions of the contribution to near-surface $[O_3]$ averaged in the afternoon during the whole episode from (a) industry, (b) residential, (c) transportation, and (d) biogenic emissions.



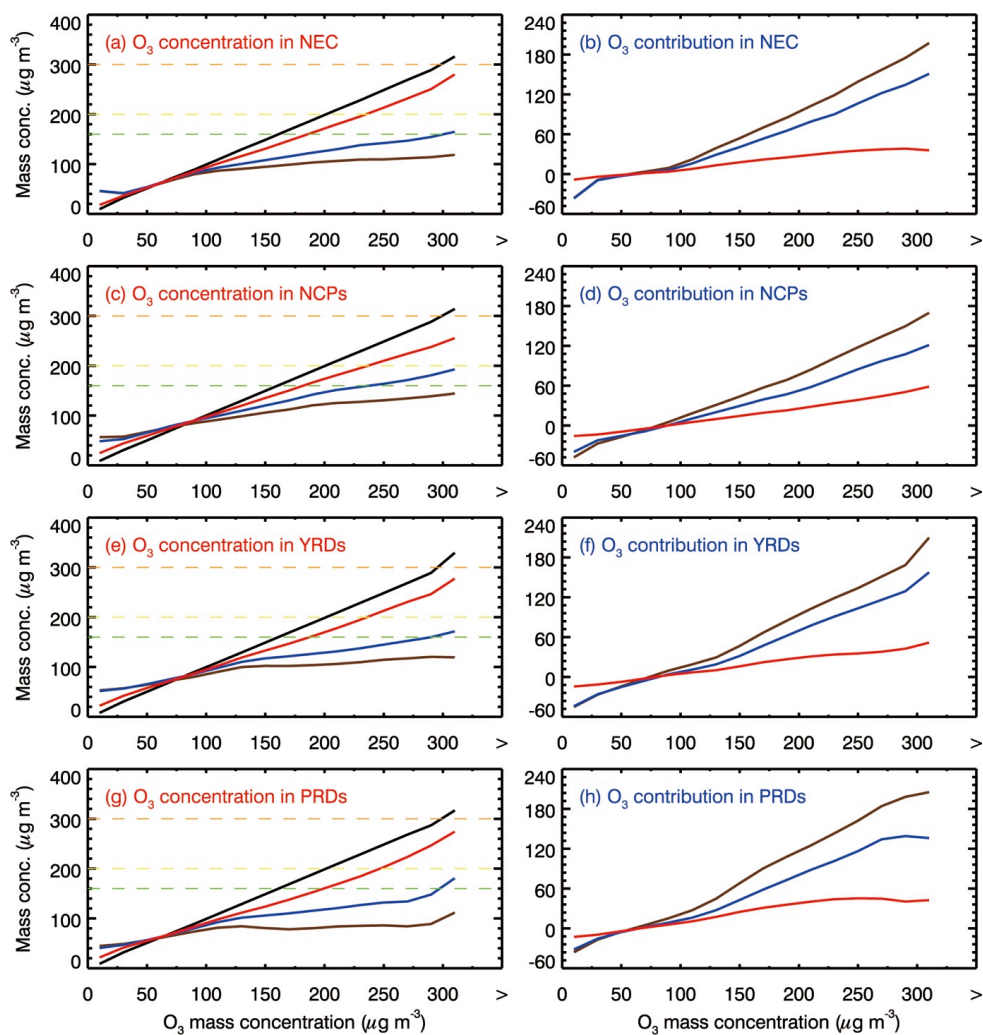
670
671
672
673
674

Figure 8 continued



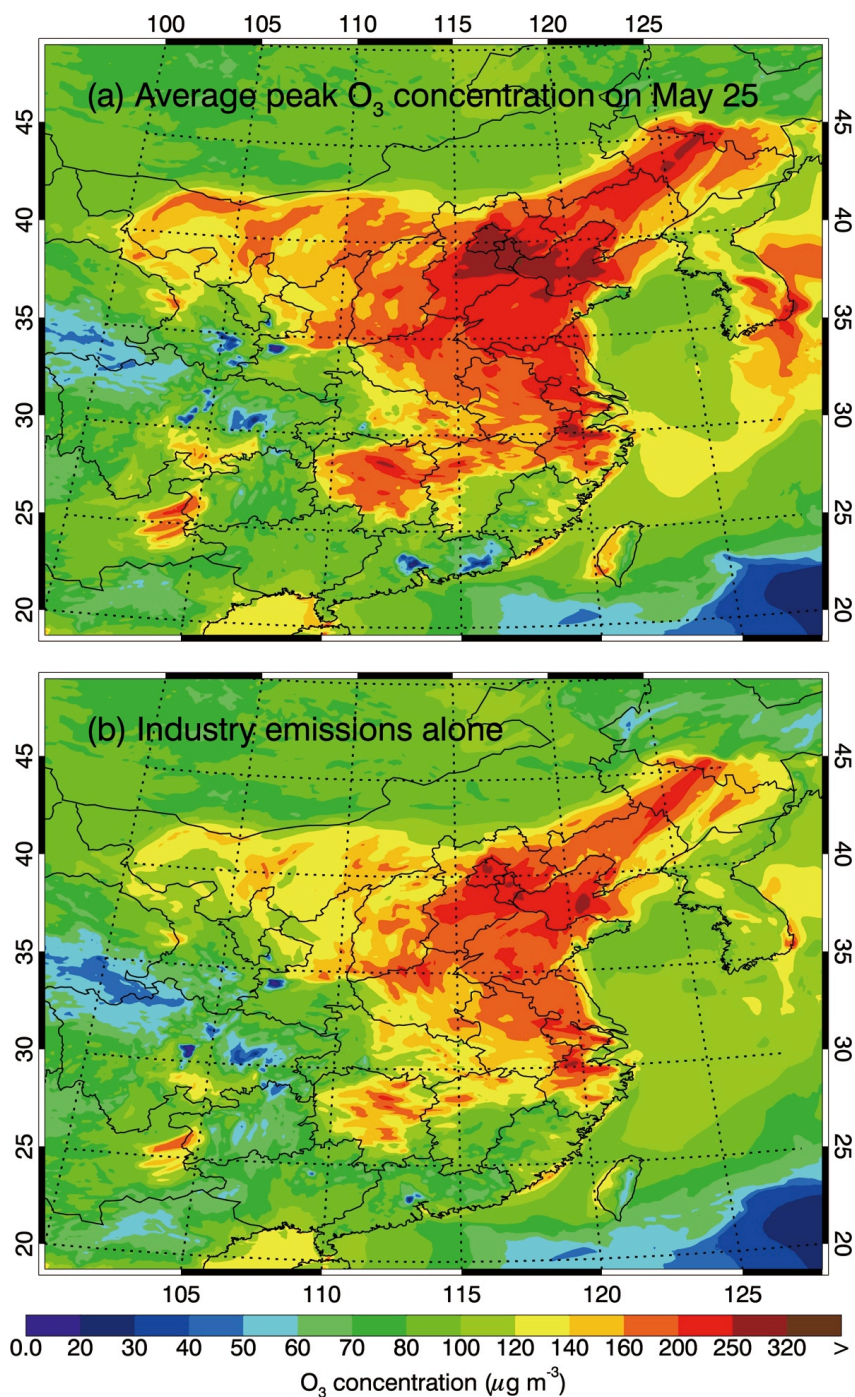
675
676
677
678
679
680

Figure 9 O₃ contributions of industry (red line), residential (brown line), transportation (blue line), and biogenic emissions (green line) in NEC, NCPs, YRDs, and PRDs, as a function of simulated [O₃] in the control case.

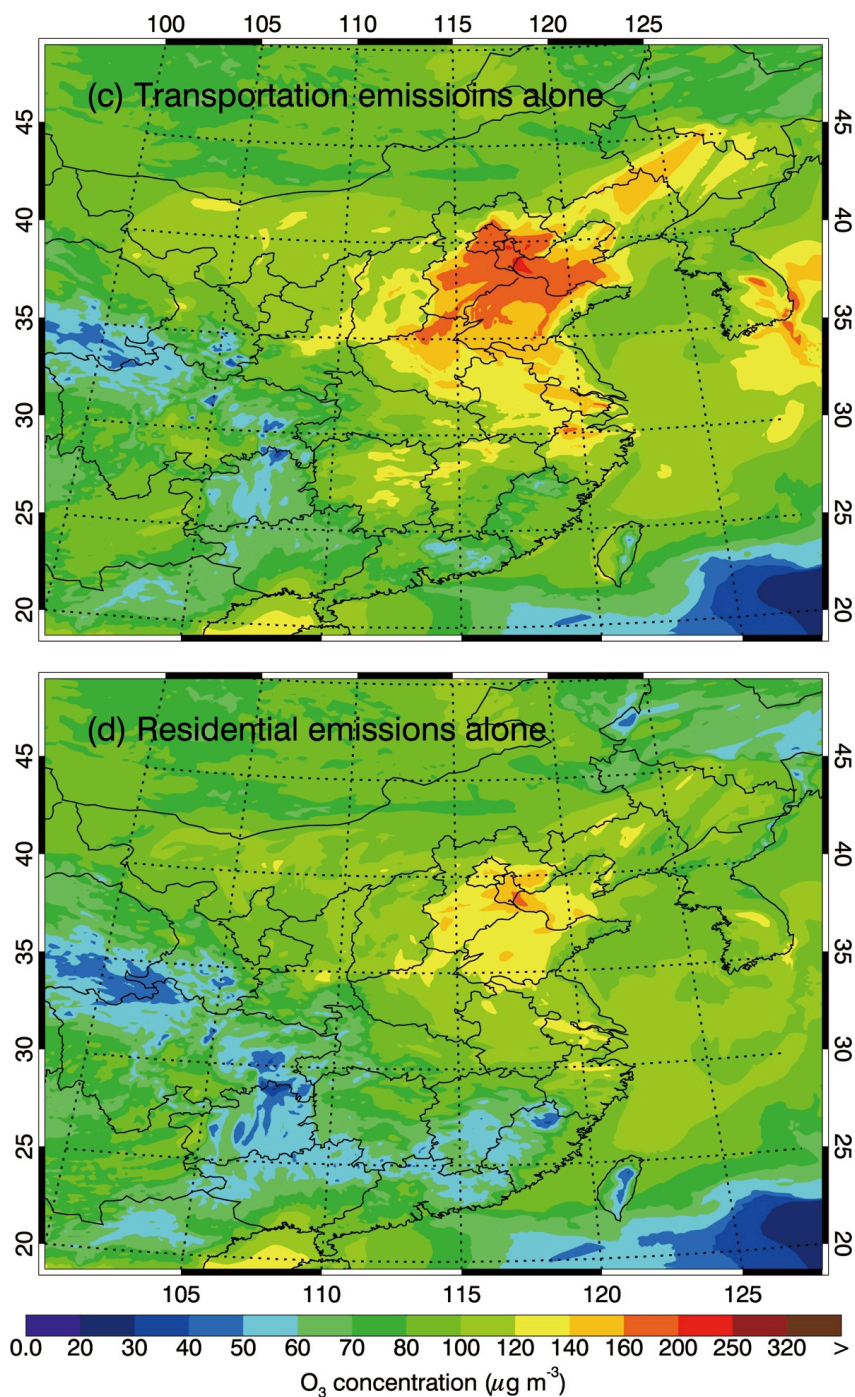


681
682
683
684
685
686

Figure 10 O₃ contributions of industry alone (red line), residential (brown line), and transportation emissions (blue line) in NEC, NCPs, YRDs, and PRDs, as a function of simulated [O₃] in the control case.



687
688
689 Figure 11 Distributions of the average O₃ concentration during peak time with (a) all
690 anthropogenic emissions, (b) industry emissions alone, (c) residential emissions alone, and (d)
691 transportation emissions alone on May 2015.



692
693
694
695
696

Figure 11 continued